Received: 7 November 2024 | Revised: 27 February 2025 | Accepted: 24 March 2025

DOI: 10.1096/fj.202402767R

RESEARCH ARTICLE

The FASEB Journal

Fibulin-4 and latent-transforming growth factor beta-binding protein-4 interactions with syndecan-2 and syndecan-3 are required for elastogenesis

Hana Hakami[1,2] | **Neha E. H. Dinesh**[1] | **Valentin Nelea**[1,3] | **Nathalie Lamarche-Vane**[1,4] | **Sylvie Ricard-Blum**[5] | **Dieter P. Reinhardt**[1,3]

[1]Faculty of Medicine and Health Sciences, Department of Anatomy and Cell Biology, McGill University, Montréal, Quebec, Canada

[2]Faculty of Sciences and Medical Studies, College of Sciences, Zoology Department, King Saud University, Riyadh, Saudi Arabia

[3]Faculty of Dental Medicine and Oral Health Sciences, McGill University, Montréal, Quebec, Canada

[4]Cancer Research Program, Research Institute of the McGill University Health Centre, Montréal, Quebec, Canada

[5]Institute of Molecular and Supramolecular Chemistry and Biochemistry (ICBMS), UMR 5246, CNRS, University Claude Bernard Lyon 1, Villeurbanne, France

Correspondence
Dieter P. Reinhardt, Department of Anatomy and Cell Biology, McGill University, 3640 University Street, Montreal, QC H3A 0C7, Canada.
Email: dieter.reinhardt@mcgill.ca

Funding information
Genetic Aortic Disorders Association Canada; Canadian Government|Natural Sciences and Engineering Research Council of Canada (NSERC), Grant/Award Number: RGPIN-2022-05045; King Saud University (KSU); Embassy of the Kingdom of Saudi Arabia in Canada; FRQ|Fonds de Recherche du Québec - Santé (FRQS), Grant/Award Number: 291220

Abstract

Elastogenesis is a cell surface-located hierarchical process that requires the core components tropoelastin and fibrillins and several accessory proteins, including fibulin-4 (FBLN4) and latent TGF-β binding protein-4 (LTBP4). FBLN4 and LTBP4 interact with cells, but their cell receptors and associated molecular elastogenic mechanisms remain unknown. Primary skin fibroblasts and several vascular smooth muscle cells bound strongly to FBLN4 multimers and LTBP4 monomers. We identified two cell interaction epitopes on FBLN4 located in cbEGF2-3 and the C-terminal domain, whereas FBLN4 multimerization sites were mapped to cbEGF4-5 and the C-terminal domain. We also determined a novel cell interaction site in the N-terminal half of LTBP4. Cell binding to FBLN4 and LTBP4 was strongly inhibited in the presence of heparin, heparan sulfate, or after enzymatic removal of heparan sulfate, suggesting heparan sulfate proteoglycans as relevant cell surface receptors. siRNA knockdown experiments identified syndecan (SDC)2 and SDC3 as cell receptors for FBNL4 and SDC3 for LTBP4. Direct protein interactions between FBLN4 and the recombinant ectodomains of SDC2 and SDC3, and between LTBP4 and SDC3 validated these results. Interaction of the elastogenic cells with FBLN4 and LTBP4 enhanced elastogenesis, whereas SDC2 and/or SDC3 knockdowns led to reduced elastic fiber formation. The cell interactions with FBLN4 and LTBP4 significantly enhanced focal adhesion formation, induced cell contraction, and led to activation of focal adhesion kinase (FAK), Erk1/2, and RhoA. Pharmacological inhibition of these effectors markedly attenuated elastic fiber formation, and siRNA knockdown of *SDC2* and *SDC3* led to reduced levels of pFAK, pERK, and active RhoA. Together, these data demonstrate that FBLN4 and LTBP4 cell interactions through SDC2 and SDC3 promote elastogenesis by enhancing focal adhesion formation, leading to cell contractility through FAK, Erk1/2, and RhoA activation, underscoring the significance of these pathways in elastogenesis.

Hana Hakami and Neha E. H. Dinesh are co-first authors.

KEYWORDS
cell contraction, cell interactions, elastic fibers, fibulin-4, focal adhesion, latent TGF-β binding protein-4, syndecan-2, syndecan-3

1 | INTRODUCTION

Elastic fibers are abundant extracellular matrix (ECM) components that confer tissues such as skin, blood vessels, and lungs with essential elastic properties for the development and survival of chordate organisms.[1] Elastic fiber formation, termed elastogenesis, takes place on or close to the cell membrane of elastogenic cells and is facilitated by the interaction of the two major components of mature elastic fibers, elastin and fibrillin-1.[2–5] Principally, tropoelastin monomers are deposited onto cell surface-associated fibrillin-containing microfibrils. The formation of nascent elastic fibers, as well as the development of mature elastic fibers comprised of an inner elastin core and an outer mantle of fibrillin-containing microfibrils, occurs through complex multistep mechanisms that require accessory proteins and enzymes. These include, but are not limited to, fibulin-4 and -5 (FBLN4/5), latent transforming growth factor beta (TGF-β) binding protein-4 (LTBP4), lysyl oxidase (LOX), LOX like-1 (LOXL1), microfibril-associated glycoprotein 4 (MFAP4), and elastin microfibril interface-located protein (EMILIN).[1,6–9] While the function of elastic fiber modifying enzymes, such as the cross-linking LOX, is well understood, the detailed molecular contributions of other accessory proteins, including FBLN4 and LTBP4, remain to be explored.

FBLN4 is a ~53 kDa short fibulin consisting of six calcium-binding EGF-like (cbEGF) domains followed by the fibulin-type C-terminus.[10] LTBP4 is a larger ~165–187 kDa multi-domain protein, consisting of two N-terminal 4-cysteine domains, one hybrid domain, and three TGF-β binding (TB) domains, interspersed between 17 cbEGF and three EGF domains.[11–13] LTBP4 occurs as two alternatively spliced isoforms, the long isoform (LTBP4L) and the short isoform (LTBP4S) that contains only one of the two N-terminal 4-cysteine domains.[11,12] Based on human mutations and knockout studies in mice, FBLN4 and LTBP4 are critical for elastogenesis. Mutations in the *FBLN4* gene lead to autosomal recessive cutis laxa (ARCL) type 1B, characterized by inelastic skin, aneurysms, arterial tortuosity, and pulmonary defects.[14–17] FBLN4 hypomorphic mice ($Fbln4^{R/R}$) are also characterized by aneurysms and arterial tortuosity.[18] Markedly, elastic fiber assembly largely fails in FBLN4 global knockout mice, which die prenatally or immediately after birth.[19] Analysis of elastic laminae in $Fbln4^{-/-}$ aortae by electron microscopy showed irregular elastic fiber aggregation and unusual rod-like filaments, indicating a major failure in elastic fiber formation.[19] Mutations in the *LTBP4* gene commonly result in ARCL type 1C, with most patients exhibiting clinical features related to elastic tissue impairment.[20–22] These include stenosis and tortuosity of pulmonary arteries, inelastic skin, as well as gastrointestinal malformations and urinary tract diverticulosis caused by tortuosity of intestinal and urinary vessels. Isoform-specific $Ltbp4S^{-/-}$ mice exhibit thinner elastic fibers in the lungs but do not entirely replicate the phenotype of human cutis laxa.[23] The more severe phenotype of the *Ltbp4* global knockout mice, lacking both LTBP4 isoforms ($Ltbp4^{-/-}$), highlighted the crucial role of LTBP4 in elastogenesis and postnatal survival.[24] This confirmed that both LTBP4 isoforms play overlapping but non-redundant roles in elastic fiber formation.

Several studies have demonstrated that FBLN4 and LTBP4 act individually and together in elastic fiber formation. For example, Noda et al. demonstrated for FBLN4 an intracellular role in the activation of pro-LOX that facilitates elastogenesis.[25] These authors showed that extracellular FBLN4 is internalized through endocytosis and interacts with pro-LOX in the trans-Golgi networks, promoting lysine tyrosylquinone formation. FBLN4 is also needed for tethering pro-LOX to tropoelastin in the ECM, facilitating elastin cross-linking.[26] Based on FBLN4's ability to bind to both, tropoelastin and fibrillin-1, it was proposed to serve as a mediator for the deposition of tropoelastin onto fibrillin-1 microfibrils.[27–29] This function also requires a direct transient interaction between FBLN4 and LTBP4, which causes a conformational change in the LTBP4 protein from a compact to an extended shape, assisting in FBLN4/tropoelastin deposition onto fibrillin-1 microfibrils.[30] The N-terminal region of LTBP4L and S can interact with FBLN4, and with FBLN5.[24,31] Also, LTBP4 serves to linearly deposit the FBLN5/tropoelastin complex onto fibrillin-1 microfibrils.[31]

We have shown that elastogenic cells interact with FBLN4 and that FBLN4 self-oligomerizes into multimers under physiological conditions, which is in turn essential for interaction with heparin.[32] It remains to be established whether FBLN4 multimerization is necessary for the interaction with cells, as well as which domain(s) are critical for oligomerization and cell binding. For LTBP4, Kantola et al. identified that recombinant human LTBP4 lacking the first two 4-Cys domains interacts with mouse lung fibroblasts at a region near the C-terminal end.[33] However,

the possibility of other cell binding sites on LTBP4 and the potential differential binding of the long and short LTBP4 isoforms are not explored. The cell surface receptors involved in mediating these interactions and the functional implications of these interactions are also elusive. Since FBLN4 and LTBP4 both lack a typical Arg-Gly-Asp (RGD) integrin binding motif, the available data suggest that heparan sulfate proteoglycans (HSPGs) on the cell surface may serve as potential cell surface receptors for these two proteins.

Syndecans (SDCs) represent one important family of cell surface heparan sulfate-containing proteoglycans. The SDC family consists of four distinct members, SDC1–4, that share similar structural domain arrangements. Each SDC contains an N-terminal ectodomain, a transmembrane domain, and a C-terminal cytoplasmic domain.[34] The ectodomain carries 3–5 heparan sulfate chains and possibly other glycosaminoglycans such as chondroitin or dermatan sulfate.[35] The domain structure is highly conserved across all syndecans in humans.[34,36,37] SDCs are transmembrane proteins that function either as homo- or heterodimers with other SDC members.[38] SDCs also display clustering, with homotypic and heterotypic interactions forming larger oligomers, particularly of SDC2.[38] The role of SDCs in elastogenesis remains insufficiently explored.

While it is clear that FBLN4 and LTBP4 play diverse vital roles in elastin fiber formation, the mechanistic requirement of FBLN4 and/or LTBP4 cell interactions in elastogenesis is not studied. Here, we have identified the cell receptors for FBLN4 and LTBP4, mapped the cell interacting domains in both proteins, and determined the consequences of these cell interactions in elastogenesis.

2 | MATERIALS AND METHODS

2.1 | Cell culture

Primary elastogenic cells from human tissues included normal skin fibroblasts (NSF), adult and fetal aortic smooth muscle cells (ASMC), umbilical arterial smooth muscle cells (UASMC), and umbilical venous smooth muscle cells (UVSMC). NSF were collected with ethics approval (PED-06-054, Research Ethics Board, Montreal Children's Hospital) from foreskin samples, and UVSMC were obtained from the American Type Culture Collection (#CRL-2481). UASMC were described previously.[32] All cells were cultured in DMEM with 10% fetal bovine serum (FBS), 100 μg/mL penicillin/streptomycin, and 2 mM L-glutamine (PSG). Fetal ASMC were purchased from ScienCell (#6110), and adult ASMC from Thermo Fisher Scientific (#C0075C). These cells were cultured in 231 Medium (Gibco; #M231500) supplemented with 10% FBS, PSG, and smooth muscle growth supplement (Gibco; #S-007-25). For recombinant protein production, HEK 293 cells and HEK 293-EBNA cells were used as described previously.[39,40] All primary and recombinant cells were cultured at 37°C in a humidified incubator under a 5% CO_2 atmosphere.

2.2 | Recombinant proteins

Full-length and several truncation and deletion fragments of human FBLN4, LTBP4L, and LTBP4S were produced as described previously.[30,32] Isoelectric points for each domain and linker region of the human LTBP4 isoforms were calculated based on their amino acid sequence (GenBank #AAC39880.2 for LTBP4L and #AAC39879.2 for LTBP4S) using the ExPASy Compute pI/Mw Tool on https://web.expasy.org/compute_pi/. Several new deletion fragments were produced for FBLN4 (F4_N1-3, F4_N1-5, F4_N1,C, F4_N1,6C, F4_N1, 4-6C and F4_4–6) and LTBP4 (L4-LN, L4-SN, and L4-C) as outlined schematically in Figures 2 and 3. The pCEP4 plasmid was used to recombinantly express all deletion mutants of FBLN4 in HEK 293-EBNA cells, and the pcDNA3.1(+) was used to produce recombinant full-length FBLN4 and all LTBP4 constructs in HEK 293 cells.[32,41,42] All recombinant plasmids were verified by DNA sequencing. The recombinantly engineered FBLN4 and LTBP4 constructs coded for a signal peptide for efficient secretion at the N-terminus and for a histidine tag to facilitate purification on their C terminus. All recombinant FBLN4 and LTBP4 proteins were purified from conditioned cell culture media by Ni^{2+}-chelating chromatography as described previously.[30,32] The purified proteins were characterized using standard SDS-PAGE, Coomassie Brilliant Blue staining, and immunoblotting with specific antibodies.[30,32] For some experiments, freshly purified full-length FBLN4 recombinant was separated into multimers, dimers, and monomers as published previously.[32]

The DNA sequences for the human syndecan ectodomains (SDC-ED2-4) were inserted into a modified episomal expression vector pCEP-Pu/BM40. Each SDC-ED construct contained the sequence coding for the BM40 signal peptide at the 5′ end of the construct, followed by an N-terminal 6-histidine tag. The sequence coding for a FLAG tag was added at the 3′ end of each SDC-ED construct prior to the stop codon. Recombinant HEK 293-EBNA cell populations were generated for each SDC-ED plasmid with culture media containing 2–6 μg/mL puromycin as a selection antibiotic. Recombinant SDC-EDs secreted into the culture medium were tested using immunoblotting and ELISA.[42]

2.3 | Dynamic light scattering

Dynamic light scattering (DLS) experiments were conducted to assess the size distribution and molecular conformation of protein particles in solution. Freshly purified recombinant proteins were analyzed in Tris–HCl, pH 7.4, 2 mM Ca^{2+} (TBS, 2 mM Ca^{2+}) buffer using the DynaPro Molecular-Sizing Instrument (Wyatt Technology, Model# DynaPro 99-E-50) and the Dynamics software (version 6) for analyses. Protein concentrations ranged from 100 to 350 μg/mL for the experiments. For each measurement, 40 acquisitions of 10 s readings were recorded and averaged. Each protein sample, derived from different batches, was measured in triplicates, and the scattering parameters were calculated based on the mean values from the 40 acquisitions. Measured hydrodynamic radii were compared to radii calculated from the protein molecular masses by applying globular (compact) and linear (extended) models for protein conformation.

2.4 | Cell binding assays

Subconfluent cells (70%–80% confluency) were briefly trypsinized, centrifuged, and washed three times in serum-free medium and then used in an endpoint and a real-time cell attachment assay. The endpoint cell binding analysis was conducted using a crystal violet cell attachment assay in 96-well Nunc plates (ThermoFisher Scientific; #439454). Wells were coated overnight at 4°C with 100 μL of 0–25 μg/mL recombinant FBLN4 (mix, multimers, dimers, monomers as described),[32] LTBP4L, LTBP4S, plasma fibronectin (pFN; positive control), and bovine serum albumin (BSA; negative control). Wells treated with TBS, 2 mM Ca^{2+} without protein were used to determine background cell binding. Wells were blocked with 2.5 mg/mL heat-denatured BSA in TBS buffer. The cells were seeded at a density of 15 000 cells/well in serum-free DMEM medium and allowed to adhere for 1 h at 37°C. After washing with TBS, the cells were fixed with 5% glutaraldehyde in TBS for 10 min and stained with crystal violet solution (0.1% in 200 mM 2-(N-morpholino) ethanesulfonic acid, pH 6) for 45 min. The dye was solubilized for 10 min in 10% acetic acid in TBS on a shaker at 500 rpm, and the absorbance was determined at 570 nm (Beckman Coulter, Model# DTX 880). To analyze cell attachment in real-time, we used an Electric Cell-Substrate Impedance Sensing (ECIS) Zθ instrument (Applied Biophysics) operated at 37°C at 5% CO_2. The cells were analyzed in ECIS 96-well plates (Applied Biophysics; #96W20idf PET). Individual wells were coated overnight at 4°C with 100 μL/well of 10 μg/mL of the proteins described above in TBS, 2 mM Ca^{2+}. Buffer alone was used as a background control. After blocking with 2.5 mg/mL heat-denatured BSA in TBS for 45 min at 37°C, the baseline was established in serum-free DMEM medium. Cells were seeded at a density of 15 000 cells per well in serum-free medium. The impedance was recorded over 4–6 h at 32 000 Hz to monitor cell adhesion and spreading (ECIS software version 1.2.186). For all cell attachment assays, the background controls were subtracted from the cell attachment values. For competition experiments, heparin and heparan sulfate were prepared as previously described.[32,43]

2.5 | Live-cell imaging

Live-cell imaging was carried out using an inverted microscope (Leica DMI6000B) equipped with a digital camera (Leica DFC365 FX Cooled B&W). Cells were maintained in a humidified incubation chamber (TOKAI, Model# HIT INU-F1 Incubator System) at 37°C and 5% CO_2 for the duration of the experiment. 24-well plates (Corning; # C3524) were coated overnight at 4°C with 300 μL/well of 25 μg/mL of FBLN4, LTBP4L, pFN, or BSA or with TBS, 2 mM Ca^{2+} as a control. After blocking with 2.5 mg/mL heat-denatured BSA for 45 min at 37°C, cells were seeded at a density of 50 000 cells per well in 500 μL medium. Imaging was conducted at 400x magnification over a 6 h period, with images captured at 30 s intervals.

2.6 | Cell-surface heparan sulfate degradation

Cells at 70%–80% confluency were harvested by a brief treatment (~3 min) with 0.05% trypsin containing 0.53 mM EDTA, followed by washing with serum-free DMEM medium and resuspension in PBS containing 1 g/L glucose, 0.1 mM $CaCl_2$, and 0.1 mM $MgCl_2$, with or without 1.25 U/mL heparinase II (Sigma;# H6512) and 0.0125 U/mL heparinase III (Seikagaku-amsbio;# EC4.2.2.8). The cell suspensions were incubated for 20 min at 37°C in a 5% CO_2 humidified incubator, with gentle shaking every 5 min to prevent cell aggregation and to ensure optimal enzyme activity. The treated cells were seeded and analyzed for cell attachment using the crystal violet cell attachment assay in protein coating conditions as described above.

2.7 | Immunofluorescence staining

For immunostaining experiments, 8-well chamber slides were prepared under protein-coated and buffer-coated

conditions. Wells were coated with specific proteins (100 µL per well, at concentrations of 10–25 µg/mL) and incubated overnight at 4°C. Wells were washed and blocked with 100 µL/well of 2.5 mg/mL heat-denatured BSA for 45 min at 37°C. Cells were typically seeded at a density of 75 000 cells per well unless specified otherwise. At the experimental endpoints, wells were washed with PBS and fixed using either 4% paraformaldehyde (PFA) for 10 min to visualize proteins in the extracellular matrix or cold 70% methanol:30% acetone for intracellular protein analysis. The cells were treated with normal goat serum (NGS) to prevent nonspecific antibody binding. Primary antibodies were incubated overnight at 4°C, followed by secondary antibodies conjugated to fluorophores (Table S1). Nuclear counterstaining was performed using 4′,6-diamidino-2-phenylindole (DAPI) at a 1:3000 dilution in NGS for 5 min, and the slides were mounted using Vectashield anti-fade medium (Vector Laboratories; #H-1000). Images were captured using a fluorescence microscope (Zeiss Axio Imager M2) and the Zen software (Zeiss, Version 2012, Blue Edition). The images were exported from the microscope in an 8-bit format. Images were processed with the ImageJ software using the previously published methodology.[44,45] To determine the FA count, images were thresholded, and the number of FAs was calculated using the *Analyze Particles* tool in ImageJ, as described previously.[40,46]

2.8 | Small interfering RNA (siRNA) knockdown experiments

All siRNAs employed in the study were purchased from Qiagen (Table S2). A cocktail of non-functional siRNAs without homology to known mammalian genes was used as a negative control for all siRNA experiments (Qiagen; All Stars siRNA). Cell transfections with 20 nM siRNAs were performed using Lipofectamine 2000 (Invitrogen; #11668500) and Opti-MEM medium (Gibco; #31985062) according to the manufacturer's instructions. Cells at 70% confluency were briefly trypsinized and washed twice with DMEM medium. 1.5×10^5 cells/mL were transfected and cultured at 37°C in a 5% CO_2 humidified incubator. The cells were harvested at different time points for cell attachment assays and immunostaining experiments.

2.9 | Real-time quantitative polymerase chain reaction (RT-qPCR)

Total RNA for gene expression analysis was extracted from cells seeded in triplicates in 12-well plates (Corning, CAT# C3513) using the Trizol method (Invitrogen; #15596018). RNA concentrations were quantified spectrometrically at 260 nm. Up to 1 µg RNA was reverse transcribed into cDNA using the ProtoScript II First Strand cDNA Synthesis Kit (New England Biolabs). Specific primers for the target genes were designed, and GAPDH was used as the housekeeping control for normalization of gene expression (Table S3). qPCR was performed using the SYBR Select master mix (Applied Biosystems) in the QuantStudio 5 Real-Time PCR System (Applied Biosystems) as previously described.[40] The data were analyzed using the Delta CT method.

2.10 | Focal adhesion formation

Cells were cultured to 50% confluency and serum-starved for 18 h. 10–50 µg/mL FBLN4, LTBP4, or pFN were coated on 8-well chamber slides and 6-well plates. Cells were seeded in serum-free DMEM medium at 15 000 cells/well in the 8-well chamber slides and 150 000 cells/well in the 6-well plates. After 24 h of incubation at 37°C with 5% CO_2, cells were washed with TBS. Cells in the 8-well chamber slides were fixed as described under "Immunofluorescence staining." Cells in 6-well plates were lysed with 50 mM Tris pH 8.0, 1 mM EDTA, 150 mM NaCl, 10% glycerol, 1% NP-40, 0.5% sodium deoxycholate, 10 mM NaF, 0.1% SDS, and 2% protease inhibitors cocktail. Protein lysates (25 µg) were separated by SDS-PAGE, followed by standard Western blotting. Anti-p-FAK (1:1000 diluted; Table S1) was used as the primary antibody, and horseradish peroxidase-conjugated goat anti-rabbit antibody (1:800 diluted) was used for detection. Blots were developed using the SuperSignal substrate (Thermo Fisher; #34580) and imaged on a ChemiDoc MP system (Bio-Rad). Band intensities were analyzed with ImageJ and normalized to GAPDH.

2.11 | Enzyme-linked immunosorbent assay (ELISA) and solid phase binding assays

For ELISA-style assays, wells in 96-well Nunc plates were coated overnight with concentrated conditioned media (0-20-fold concentrated) containing the soluble recombinant FLAG-tagged SDC2-ED, SDC3-ED, or SDC4-ED. For solid phase binding assays, the 96-well plates were first coated with 10 µg/mL recombinant FBLN4, LTBP4L, LTBP4S, pFN, or BSA (100 µL/well, each in TBS, 2 mM Ca^{2+}) and then incubated with the concentrated conditioned media. Detection of the FLAG-tagged SDC2-ED,

SDC3-ED, or SDC4-ED in the wells coated with conditioned medium (Figure 6B) or of these proteins bound to the precoated recombinant proteins (Figure 6C–G) was performed with a specific anti-FLAG tag primary antibody (1:1000 diluted), followed by incubation with the horseradish peroxidase-conjugated secondary antibody (1:800 diluted) (Table S1). Color development was performed with 1 mg/mL 5-aminosalicylic acid in 20 mM phosphate buffer, 0.045% H_2O_2, pH 6.8 while shaking at 500 rpm. The reactions were stopped with 2 M NaOH, and the absorbance was determined at 492 nm. Signals were corrected for antibody cross-reactivity with the coated ligands and for nonspecific interactions of the soluble ligands with wells treated only with TBS, 2 mM Ca^{2+}.

2.12 | Collagen gel contraction assay

Commercial rat tail collagen type I solution was used to generate disk-shaped gels for contraction assays (Cultrex, R&D Systems; #3440-100-01). Confluent cells were trypsinized, washed with serum-free DMEM medium, and resuspended in DMEM containing 10% pFN-depleted serum prepared as described previously.[47] The cell suspension was supplied with 10 µg/mL FBLN4, LTBP4L, pFN, or TBS/2 mM Ca^{2+}. A total of 250 µL cell suspension containing 5×10^5 cells/mL was mixed with 250 µL collagen type I solution, yielding a final collagen concentration of 1.5 mg/mL. Non-cellularized control gels were prepared with DMEM only. The pH of the collagen-DMEM solution was adjusted to 7.2 using 1 M NaOH. The mixture was transferred to a 24-well plate and allowed to polymerize for 1 h at ambient temperature. The solidified gels were detached from the wells using a spatula, and 500 µL of medium was added to each well. The gels were incubated in a humidified incubator at 37°C and 5% CO_2 for 7 d. Images were recorded daily using a gel imaging system (Bio-Rad; ChemiDoc MP Imaging system). The area of the contracted gels was determined using ImageJ.

2.13 | Cell Contraction inhibition analysis

Cell contraction inhibition was performed with 50 µM blebbistatin and an inactive blebbistatin control (Millipore; #203392, #203390). 0.01% DMSO served as a control in all inhibition experiments. The medium containing the blebbistatin or the control was changed every 3 d for all experiments. The experimental conditions for inhibition of collagen gel contraction were identical to those described above, except that the treatment period with active blebbistatin or the inactive control was 14 d. To analyze the impact of cell contraction inhibition on elastogenesis, NSF were seeded at 75 000 cells per well in 8-well chamber slides as described under "Immunofluorescence staining". The cells were treated with active blebbistatin and the inactive control for 7 d. Immunostaining of alpha-smooth muscle actin (αSMA) and tropoelastin was performed as described under "Immunofluorescence staining".

2.14 | FAK/ERK/RhoA inhibition analysis

NSF were seeded onto protein-coated and non-coated 8-well chamber slides as described under "Immunofluorescence staining". 24 h after seeding, the medium was replaced with DMEM containing either 0.1% DMSO as control, or one of the following inhibitors: 10 µM FAK inhibitor PF573228 (Selleckchem; #S2013), 10 µM ERK inhibitor SCH772984 (Selleckchem; #S7101), or 1 µM RhoA inhibitor CCG-1423 (Selleckchem; #S7719). Cells were cultured for 5 d under these conditions, fixed using a methanol-acetone solution (70:30 ratio), and immunostained for tropoelastin using specific antibodies (Table S1) as described under "Immunofluorescence staining".

2.15 | Surface plasmon resonance spectroscopy (SPR)

SPR was performed to determine the interaction kinetics of the SDC-EDs (Biacore X; Cytiva). FBLN4, LTBP4L, and LTBP4S were immobilized on one flow channel of CM5 sensor chips by standard amine coupling (400–600 RU). The second flow channel of the sensor was left blank and used as a control. 20-fold concentrated conditioned media containing SDC-EDs were applied at 10 µL/min for 180 s (association) in TBS, 2 mM Ca^{2+}. Kinetic analyses were performed by monitoring dissociation for 600 s. The dissociation rate constants k_d were determined by fitting the experimentally obtained dissociation curves (BIAevaluation software).

2.16 | Statistics

All statistical analyses of the quantified data and the graphs were performed using Origin software (Origin Lab Corporation, version 9.6.0.1722019). Student *t*-test and ANOVA (analysis of variance) were used to calculate the *p*-values. The selection of the appropriate statistical test was made for individual sets of experiments according to the data distribution, the independence of variables, as

well as the number of variables and sample groups in a comparison. *P*-values ≤0.05 were considered statistically significant.

3 | RESULTS

3.1 | FBLN4 multimerization is essential for cell interactions, and LTBP4 isoforms interact similarly with elastogenic cells

Cell interaction with FBLN4 mono-, di-, and multimers (prepared as described previously)[32] and with the two LTBP4 isoforms LTBP4L and LTBP4S was tested with primary normal human skin fibroblasts (NSF) using endpoint crystal violet staining (Figure 1A) and real-time Electric Cell-Substrate Impedance Sensing (ECIS) (Figure 1B). NSF interacted strongly with FBLN4 multimers isolated by gel filtration,[32] similar to the non-gel filtrated FBLN4 preparation that consisted of a mix of multimers, dimers, and monomers. FBLN4 dimers showed weak interactions in the crystal violet assay and no interaction in the ECIS approach, whereas FBLN4 monomers were completely inactive in cell adhesion. Both LTBP4L and S interacted strongly and similarly with NSF.

We previously demonstrated the interaction of recombinant FBLN4 with elastogenic cells such as lung and skin fibroblasts and umbilical arterial and venous smooth muscle cells (UASMC and UVSMC, respectively).[32] Here, we compare the interactions of FBLN4 and LTBP4L with these cells and broaden the scope by assessing their binding to adult and fetal aortic smooth muscle cells (ASMC). All primary cells showed strong and similar binding to FBLN4 and LTBP4L, comparable to the positive control (pFN) (Figure 1C). Since smooth muscle cells can be in a contractile or synthetic state, we evaluated whether the differentiation status affected the ability to interact with FBLN4 and LTBP4L.

Cell attachment and spreading of skin fibroblasts on FBLN4- and LTBP4L-coated surfaces were analyzed by live-cell imaging from 2 min to 6 h post-seeding (Figure 1D). Fibroblasts adhered rapidly to FBLN4- and LTBP4-coated surfaces, with initial attachment observed within 2 min, similar to the positive control (pFN). In contrast, cells seeded on non-coated surfaces showed poor adhesion (Figure 1D). Immunostaining of αSMA revealed fibroblast spreading on FBLN4- and LTBP4-coated surfaces, comparable to pFN-coated surfaces at 1 h post-seeding (Figure 1E, Top panel). At 4 h, the cells were well spread across all protein-coated surfaces (Figure 1E, Bottom panel). No cell spreading was apparent on non-coated surfaces. A significant increase in αSMA levels suggested enhanced stress fiber formation under protein-coated conditions (Figure 1F).

3.2 | Identification of multimerization and cell binding domains in FBLN4

We previously identified two self-oligomerization sites on FBLN4 at cbEGF2-5 and cbEGF6-Cterm.[30] To further refine these self-oligomerization regions and identify the specific cell interaction sites on FBLN4, we generated several recombinant FBLN4 truncation and deletion mutants using HEK-EBNA cells (Figure 2A). All constructs included a signal peptide for secretion and post-translational modification in the secretory pathway and a C-terminal histidine tag to facilitate purification. Recombinant proteins were purified from conditioned cell culture medium by Ni^{2+}-chelating chromatography and analyzed by SDS-PAGE (Figure 2B). Full-length FBLN4 and the non-overlapping F4_N1, F4_2–5, and F4_6C were previously characterized in detail.[30,32] All new recombinant FBLN4 mutant proteins migrated at the expected molecular mass under reducing conditions (arrowheads in Figure 2B; calculated masses are indicated). Double bands at the monomeric position of some fragments likely represent differential glycosylation as determined previously for full-length FBLN4.[32] Under non-reducing conditions, most FBLN4 mutants, except F4_N1-3, showed various levels of multimerization. F4_N1-3, F4_N1-5, and F4_N1,C showed an estimated purity of >90%; F4_N1,6C and F4_N1,4-6C were about 40–50% pure, but F4_4–6 could only be enriched to an estimated 10%–15% purity. Additional purification steps did not improve the purity because of the relatively low abundance of recombinant protein in the conditioned medium. To properly control those partially purified FBLN4 fragments in cell binding assays, a conditioned medium was prepared from non-transfected HEK-EBNA cells and subjected to the same chromatographic purification scheme used for the FBLN4 deletion mutants. This preparation contained the co-purified proteins and could thus serve as a background control.

Multimerization of purified proteins was evaluated by dynamic light scattering (DLS) analysis, which provides information on the hydrodynamic radius of proteins and thus on the molecular masses of monomers and multimers in solution (Figure 2C). We have previously shown that F4_N1 produced a single monodisperse population of particles with a hydrodynamic radius of 2.5 nm, representing monomers.[30] F4_N1-3 containing two additional downstream cbEGF domains, analyzed in the present study, also showed preferentially a population of particles with a hydrodynamic radius of 3 nm. These data demonstrate that the N-terminal FBLN4 domain and the two downstream cbEGF domains are not able to multimerize. All other FBLN4 truncation and deletion mutants exhibit multimerization with a major peak between 7.2–15.0 nm and a minor peak between 80 and 100 nm. These data are

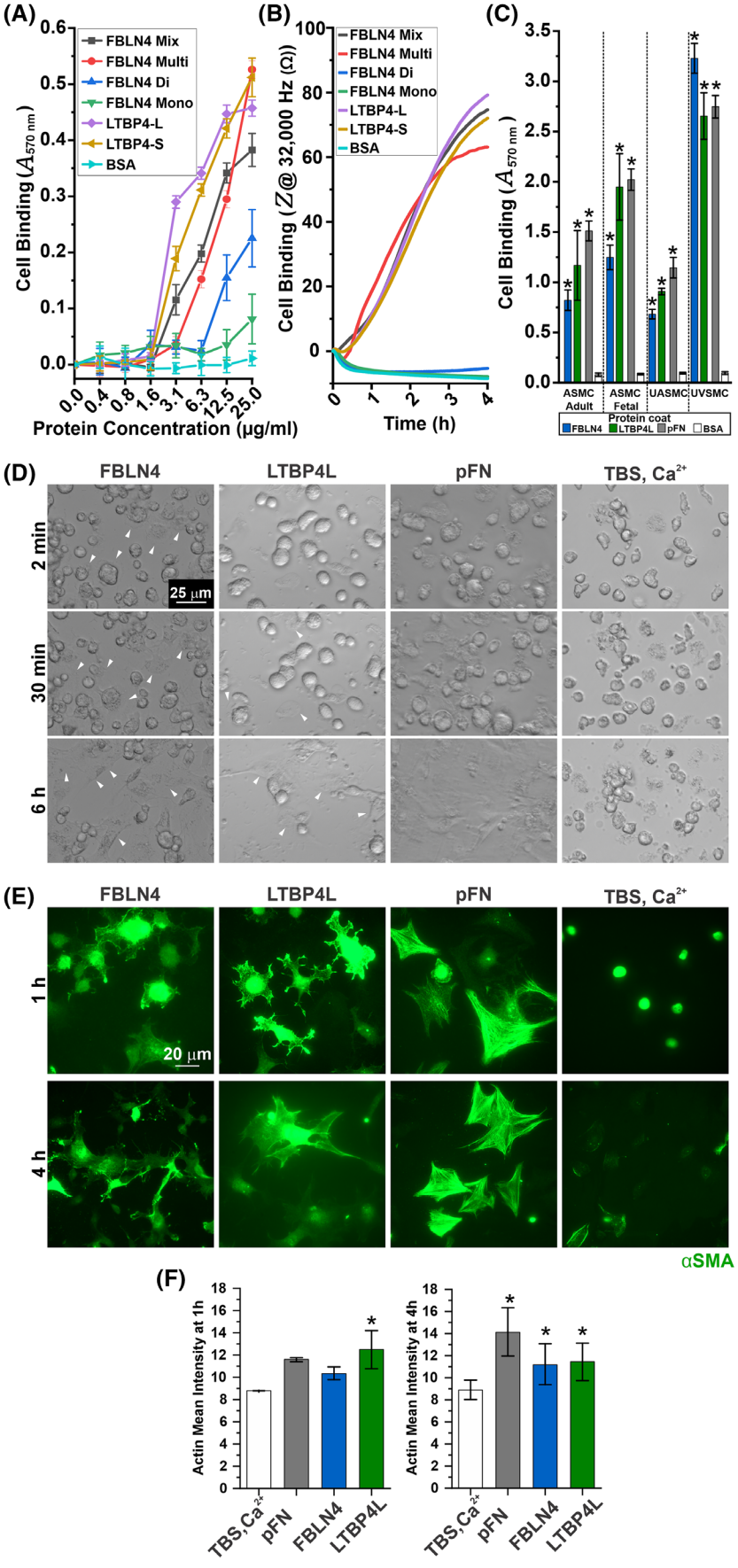
(A)
FBLN4 Mix
FBLN4 Multi
FBLN4 Di
FBLN4 Mono
LTBP4-L
LTBP4-S
BSA
Cell Binding ($A_{570\ nm}$)
Protein Concentration (μg/ml)
(B)
Cell Binding (Z@ 32,000 Hz (Ω))
Time (h)
(C)
Cell Binding ($A_{570\ nm}$)
ASMC Adult
ASMC Fetal
UASMC
UVSMC
Protein coat
FBLN4 LTBP4L pFN BSA
(D)
FBLN4
LTBP4L
pFN
TBS, Ca2+
2 min
30 min
6 h
25 μm
(E)
1 h
4 h
20 μm
αSMA
(F)
Actin Mean Intensity at 1h
Actin Mean Intensity at 4h
TBS,Ca2+
pFN
FBLN4
LTBP4L

FIGURE 1 Cell interactions with FBLN4 and LTBP4. (A, B) The graphs show NSF interactions with immobilized recombinant FBLN4 multimers (Multi), dimers (Di), and monomers (Mono) purified by gel filtration, as well as non-gel filtrated FBLN4 (Mix), and LTBP4L and LTBP4S isoforms using a crystal violet endpoint assay in (A) and an ECIS real-time assay in (B). In A, proteins were coated at the indicated concentrations; in B, the protein coating concentration was 10 μg/mL. The cell binding data represent averaged quadruplicates of a representative experiment. The experiment was repeated 5–6 times using NSF from 4 donors. BSA was used as a negative control. Background cell binding in the buffer control (TBS, 2 mM Ca^{2+}) was subtracted from all other values. Error bars indicate standard deviation. (C) Crystal violet endpoint cell binding assay to analyze FBLN4 (blue) and LTBP4L (green) interactions with different smooth muscle cells: adult and fetal aortic SMC (ASMC), umbilical aortic SMC (UASMC), and umbilical venous SMC (UVSMC). pFN (gray) represents a positive control, and BSA (white) the negative control. All samples were compared to the BSA control for statistical analyses. Error bars represent standard deviation of 3–4 replicates of one representative experiment (4 experiments total). (D) Differential interference contrast microscopy images obtained from live cell fibroblast adhesion and spreading (arrowheads) on FBLN4, LTBP4L, and pFN-coated wells and the TBS, Ca^{2+} buffer control at the time after seeding as indicated ($n = 3–5$ per protein). The scale bar represents 25 μm. (E) Representative images of αSMA immunostaining of NSF at 1 and 4 h after seeding on FBLN4, LTBP4L, or pFN-coated wells, and the TBS, Ca^{2+} buffer control ($n = 3$). Note that cell spreading was observed under FBLN4, LTBP4L, and pFN-coated conditions by 1 h. (F) Quantification of αSMA immunostaining in (E). The scale bar represents 20 μm. Statistical analyses were performed using the unpaired Student's two-tailed *t*-test. * Indicates statistical significance with *p*-values ≤.05.

consistent with the SDS-PAGE analyses of the fragments under non-reducing conditions (Figure 2B), narrowing down the multimerization domains in FBLN4 map to cbEGF4-5 and to the C-terminus, potentially a contiguous site in this region.

To identify the FBLN4 domains involved in cell interactions, we analyzed mutant and full-length FBLN4 in cell binding assays using NSF (Figure 2D). The deletion mutants F4_N1 and F4_4-6 displayed no cell interaction, whereas mutant fragments containing either cbEGF2-3 or the C-terminal domain interacted strongly with cells. These two cell interaction sites are under physiological conditions sufficiently positively charged (cbEGF2-3, pI = 7.8; C-terminal domain, pI = 9.2) to mediate cell interactions via negatively charged heparan sulfate cell surface receptors, as predicted previously.[32]

3.3 | Identification of a novel cell binding site in the LTBP4 N-terminal region

Kantola et al. previously discovered one cell binding region near the C-terminus of LTBP4, using the full-length LTBP4S isoform and several smaller fragments (Figure 3A).[33] To compare cell interaction between the LTBP4L and LTBP4S isoforms, and to potentially identify additional cell interaction sites that were previously missed, we have produced recombinant LTBP4L and LTBP4S as well as the N- and C-terminal halves of both LTBP4 isoforms (Figure 3A). LTBP4L and the recombinant halves could be readily purified in sufficient amounts, whereas LTBP4S was more difficult to obtain. Therefore, some of the following experiments could not be conducted with LTBP4S. The purified proteins were analyzed by SDS-PAGE under reducing and non-reducing conditions (Figure 3B,C), and characterized by DLS for possible multimerization (Figure S1A). Full-length LTBP4L and LTBP4S migrated at ~200 kDa under reducing conditions, which was higher than the calculated molecular masses of 173.5 kDa (LTBP4L) and 165.9 kDa (LTBP4S), likely due to the contribution of the N-glycans. Full-length LTBP4 isoforms analyzed by DLS showed the presence of primarily monodisperse populations of particles with hydrodynamic radii of 8.4 nm for LTBP4L and 7.5 nm for LTBP4S, demonstrating that the full-length proteins did not multimerize in solution. The N-terminal recombinant half of each isoform migrated at ~100 kDa, which was also higher than the calculated values of 88.4 kDa for L4-LN and 80.9 kDa for L4-SN. These N-terminal halves displayed hydrodynamic radii of 25.4 nm (L4-LN) and 20.8 nm (L4-SN), demonstrating that both are present as multimers in solution (Figure S1A). The ability to multimerize is possibly due to the unmasking of a multimerization site in the absence of the C-terminal half. Both N-terminal halves showed minor bands of ~60 kDa under reducing conditions, which likely represent proteolytic cleavage products. The common C-terminal half migrated at ~130 kDa in SDS-PAGE and showed a monodisperse particle population in DLS with a hydrodynamic radius of 6.8 nm, demonstrating that this fragment is monomeric in solution.

Cell binding of the purified full-length and deletion mutants of both LTBP4 isoforms was tested using the crystal violet assay with NSF (Figure 3D). The cells bound strongly and similarly to full-length LTBP4L and LTBP4S. In addition, the fibroblasts adhered strongly to all three deletion constructs at about 75% compared to the full-length proteins. As the N- and the C-terminal halves did not contain overlapping domains, the data demonstrate that both LTBP4L and LTBP4S contain at least two independent cell interacting sites, one novel binding site located in the N-terminal half and the other in the C-terminal half, as previously shown.[33]

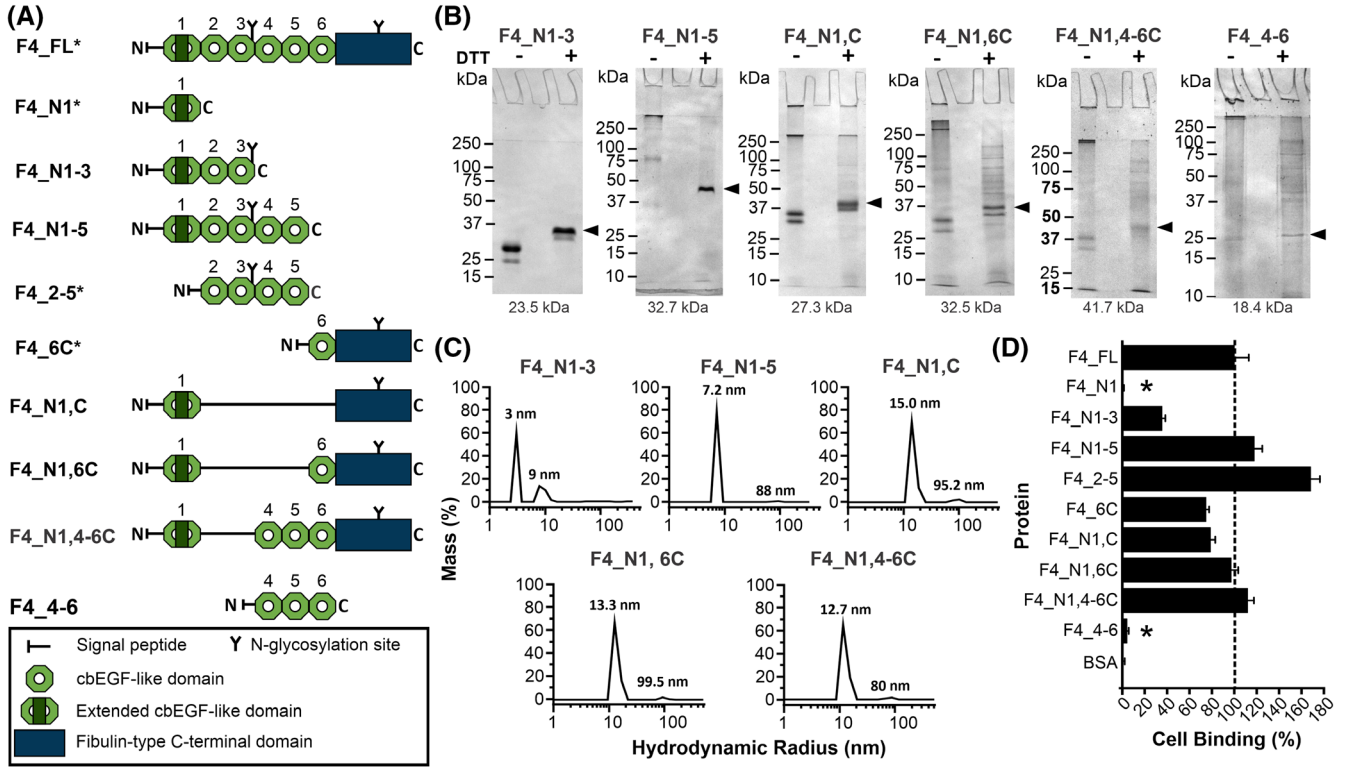

FIGURE 2 Mapping of multimerization and cell interaction sites on FBLN4. (A) Schematic presentation of the domain arrangement of human full-length FBLN4 (F4_FL) and all FBLN4 truncation and deletion mutants recombinantly produced and used in this study. Proteins marked by asterisks were produced in previous studies.[30,32] All proteins were constructed with a signal peptide at the N terminus and with a histidine tag at the C-terminal ends. (B) SDS-PAGE of the newly constructed and purified recombinant FBLN4 deletion mutants. Molecular masses indicated under each gel were calculated theoretically based on the amino acid composition. Arrowheads indicate the respective protein bands. (C) DLS analyses of recombinant FBLN4 mutants to determine monodispersity and multimerization. The graphs show the hydrodynamic radius in nm on a logarithmic scale on the *X*-axis versus the mass (%) on the *Y*-axis. (D) Crystal violet cell binding assay to analyze NSF interactions with FBLN4 full-length and deletion constructs. Wells coated with BSA were used as a negative control. Error bars represent the standard deviation of 3 replicates of one representative experiment (5 experiments in total using NSFs from 3 different donors). Full-length FBLN4 was set to 100% binding, and all samples were compared to full-length FBLN4 for statistical analyses. Statistical analyses were performed using two-way ANOVA. * Indicates statistical significance with *p*-values ≤.05.

This correlates with the presence of three domain clusters with basic isoelectric points. One cluster is located in the N-terminal 4-Cys domains of both isoforms, the second in the region including the first TB domain and two downstream EGF domains, and the third in the linker regions adjacent to the second TB domain (Figure 3A). The presence of these basic clusters represents candidate regions for interactions with cell surface heparan sulfate receptors.

3.4 | Cell interactions with FBLN4 and LTBP4 isoforms are not dependent on integrins

Several cell surface receptors, including heparan sulfate proteoglycans (HSPG) and integrins, mediate interactions with ECM proteins. We first screened the primary fibroblasts and smooth muscle cells used in this study for mRNA expression of HSPGs and integrins by real-time qPCR, which was subsequently translated into a heat map (Figure 4A). *SDC2-4* and *GPC2-6* mRNAs were expressed at various levels across the tested cell types, but not *SDC1* and *GPC1*. Several of the tested integrin mRNAs were also expressed across all examined elastogenic cells, whereas *ITGA2B* and *ITGA7-9* were not expressed, and *ITGB2*, *ITGB4*, and *ITGB7* were only expressed by some cells.

Interactions of ECM proteins with integrins require divalent cations, including Ca^{2+}, Mg^{2+}, and Mn^{2+} that bind to the α and β integrin subunits.[48] To test the possibility of integrin involvement in FBLN4 and LTBP4 cell interaction, we used serial titrations of the divalent cation chelator EDTA and selected metal cations in the cell binding buffer (Figure 4B–E). Cells lost ~70%–80% of their ability to attach to the pFN and tropoelastin control in the presence of ~1.5 mM EDTA. On the contrary, cell adhesion to FBLN4

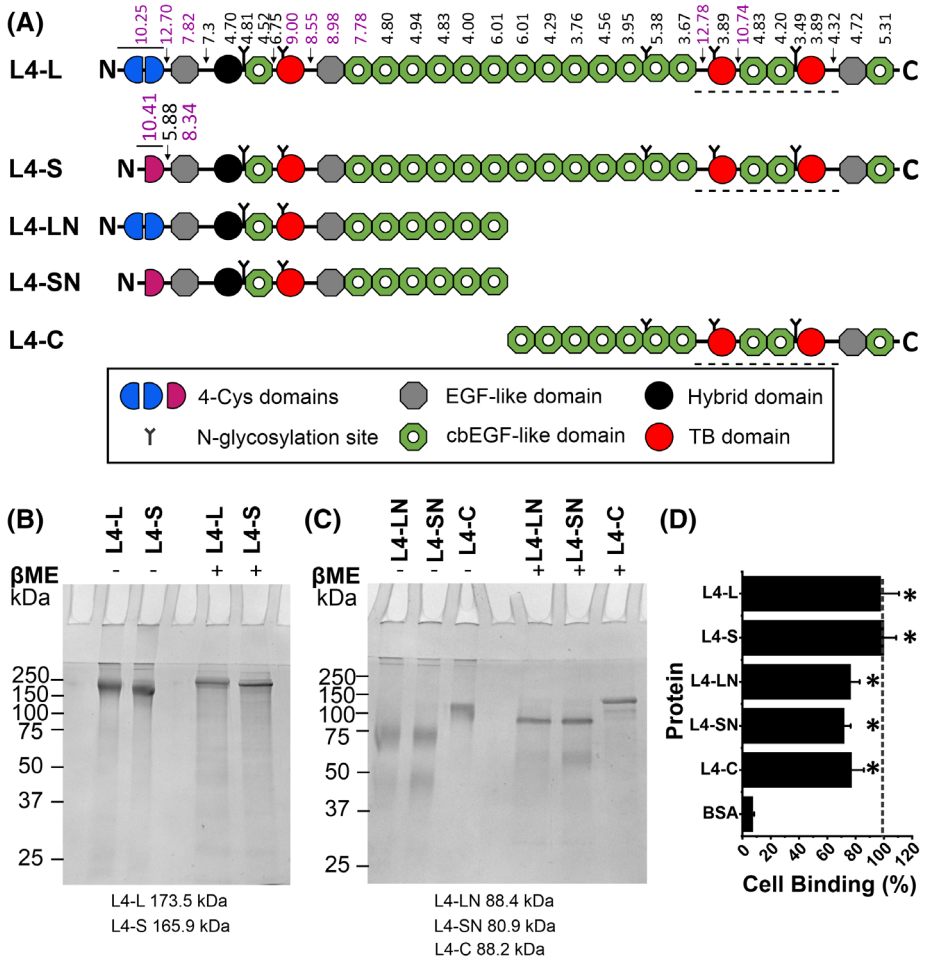

FIGURE 3 Identification of a novel cell binding site at the N-terminal half of LTBP4 isoforms. (A) Domain structure of full-length human LTBP4 long and short isoforms (L4-L and L4-S, respectively) and the LTBP4 truncation mutants. All LTBP4 recombinant proteins were constructed with the endogenous signal peptide except the C-terminal half (L4-C) which was constructed with the BM40 signal peptide at the N-terminus. Isoelectric points for each domain and linker region (arrows) are indicated above L4-L. The isoelectric points for the domains with 100% identical amino acid sequences between the long and the short form are indicated only above the long form schematic. Basic isoelectric values are magenta colored. The dashed lines indicate the previously mapped cell binding region identified by Kantola et al.[33] (B, C) Purified recombinant LTBP4 full-length and deletion mutants analyzed under non-reducing (−βME) and reducing (+βME) conditions by SDS-PAGE. Calculated molecular masses of the recombinant proteins are indicated below the gel images. Molecular masses of marker proteins are indicated on the left. (D) Cell interaction of the recombinant LTBP4 proteins with NSF. BSA was used as a negative control, and all samples were compared to BSA control for statistical analyses. Error bars represent the standard deviation of 3 replicates of one representative experiment (3 experiments total). Statistical analyses were performed using two-way ANOVA. * Indicates statistical significance with p-values ≤.05.

and LTBP4 was reduced only by about 10%–20% at much higher EDTA concentrations of ~25 mM. At 100 mM EDTA, cell interactions to all tested proteins were completely lost (Figure 4B). The data indicate that divalent cations were removed from integrins by relatively low EDTA concentrations, resulting in the loss of integrin-dependent pFN or tropoelastin cell interaction. However, FBLN4 and LTBP4 likely bind to other cell surface receptors and possibly lose their ability to interact with cells upon removal of divalent cations by high EDTA concentrations from cbEGF domains present in both proteins. To exclude possible direct EDTA effects on FBLN4 and LTBP4 cbEGF domains, NSF were pretreated with EDTA to remove cations from integrins and then tested after EDTA removal for cell binding with Ca^{2+}-saturated FBLN4, LTBP4, pFN, and tropoelastin in the presence of increasing concentrations (0–4 mM) of Ca^{2+}, Mg^{2+} or Mn^{2+} (Figure 4C–E). pFN and tropoelastin showed a strong dependency of cell binding on increasing concentrations of all tested divalent cations, strongly supporting the cognate integrin-dependent interactions with these proteins. However, FBLN4, LTBP4L, and LTBP4S remained at a similar cell binding level, irrespective of available cations, strongly suggesting that FBLN4, LTBP4L, and LTBP4S interact with cells in an integrin-independent manner.

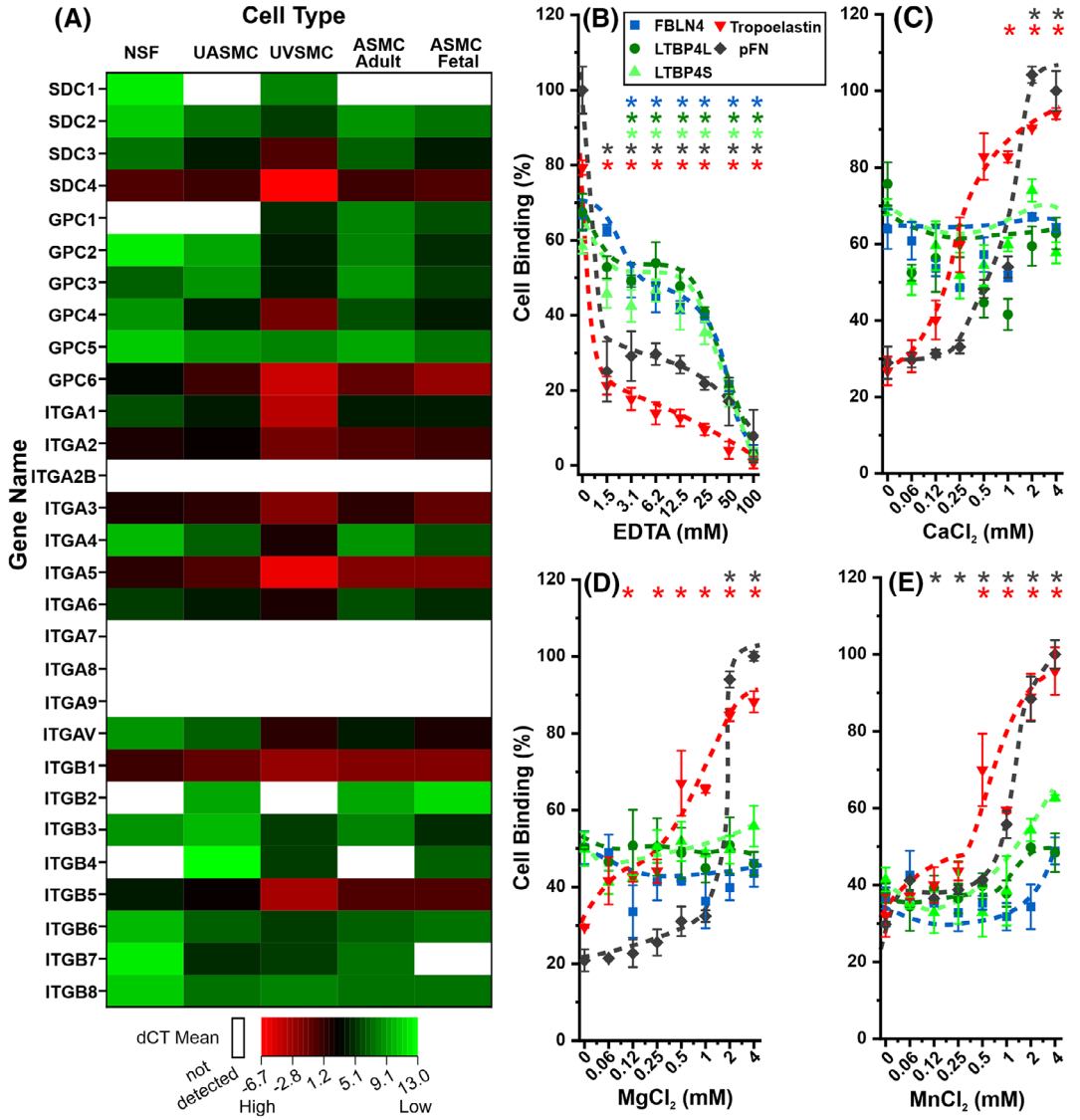

FIGURE 4 Cell surface receptor profiling and cation dependency of FBLN4 and LTBP4 cell interactions. (A) mRNA expression profiling of cell surface receptors on human elastogenic cells. The heatmap shows mRNA expression data of cell surface receptors commonly interacting with ECM proteins obtained from real-time qPCR analyses using primary human skin fibroblasts (NSF), umbilical aortic SMC (UASMC), umbilical venous SMC (UVSMC), and adult and fetal aortic SMC (ASMC). Data in the heatmap are presented for each mRNA (rows) and each cell type (columns). Expression values are presented as ΔCT after normalization to GAPDH. Black blocks indicate that mRNA expression levels of the respective receptor and GAPDH have the same value. If the mRNA level is lower than that of GAPDH, the blocks are green; if the level is higher, they are depicted in red. White blocks indicate that no mRNA expression was detected. (B–E) Shown are representative cell binding assays using NSF tested with FBLN4, LTBP4L, LTBP4S, tropoelastin, and pFN. (B) The assay was performed in the presence of 0–100 mM EDTA in the binding buffer. (C–E) Skin fibroblasts were first preincubated in 5 mM EDTA, then washed and used in the assay in the presence of 0–4 mM divalent cations in the cell binding buffer, including Ca^{2+} (C), Mg^{2+} (D) and Mn^{2+} (E). The value for the positive control pFN was set to 100%. Error bars represent the standard deviation of 4 replicates of one representative experiment (3 experiments total). Statistical analyses were performed using two-way ANOVA. Significant differences ($p < .05$) are indicated by color-coded asterisks matching the colored graphs. * Indicates statistical significance with p-values ≤.05.

3.5 | Cell surface heparan sulfate and syndecans mediate FBLN4 and LTBP4 cell interactions

To test whether FBLN4 and LTBP4 cell interactions are heparan sulfate dependent, competitive cell binding assays were conducted in the presence of soluble heparin or heparan sulfate in the binding buffer (Figure 5A,B). Cell binding to FBLN4 and to LTBP4L was significantly reduced by the presence of 25–50 μg/mL heparin and completely blocked at 100 μg/mL heparin (Figure 5A). Similarly, FBLN4 and LTBP4L cell adhesion was significantly

reduced in the presence of 25–100 μg/mL heparan sulfate (Figure 5B). These data narrow down the cell surface receptors for FBLN4 and LTBP4L to HSPGs.

To explore whether the binding moiety to FBLN4 and LTBP4 on cells is indeed heparan sulfate side chains of a proteoglycan, NSF was first treated with heparinases to degrade cell surface heparan sulfate chains and then tested for cell binding to FBLN4 and LTBP4L (Figure 5C,D). We combined heparinases II and III (H'ase II & III) to ensure optimal cleavage of heparan sulfate chains from proteoglycans on the cell surface. Immunostaining using a heparan sulfate-specific antibody revealed effective degradation of the heparan sulfate chains (Figure 5C). Treatment of NSF with heparinases II and III significantly diminished cell binding to FBLN4 and LTBP4L by about 50% (Figure 5D). These data demonstrate the critical involvement of heparan sulfate in FBLN4 and LTBP4 cell interactions.

To identify the HSPG acting as FBLN4 and LTBP4 receptors, we employed global siRNA knockdown of syndecans and glypicans. Since we observed that SDC1 and GPC1 were not expressed by all cell types that interacted with FBLN4 and LTBP4 (Figure 4A), we excluded these two HSPGs from the siRNA knockdown analysis. NSF were transfected with a cocktail of siRNA against SDC2-4 or GPC2-6, or with scrambled siRNA without any mammalian target sequences as a negative control in all siRNA knockdown experiments. After siRNA transfection, cells were analyzed for mRNA expression of the target genes to confirm siRNA knockdown and tested for binding to immobilized FBLN4 and LTBP4. For both pools, SDC2-4 and GPC2-6, we observed an almost complete reduction of the respective HSPG mRNA versus the scrambled controls (Figure 5E,F). Knockdown of SDC2-4 inhibited cell binding to FBLN4 and LTBP4L, whereas GPC2-6 knockdown did not (Figure 5G). These data demonstrate that one or more of SDC2-4 mediates cell interactions with FBLN4 and LTBP4.

To identify the syndecan isoforms on elastogenic cells that interact with FBLN4 and both LTBP4 isoforms, we performed individual siRNA silencing of *SDC2*, *3*, or 4 mRNA expression. First, NSF were transfected with SDC-specific siRNAs and then validated for siRNA knockdown efficiency and specificity (Figure 5H). Consistent with the previous siRNA knockdown analysis, after siRNA transfection, we observed a significant and almost complete reduction in the mRNA expression levels of *SDC2*, *SDC3*, and *SDC4*. We commonly noted that knocking down an individual *SDC* mRNA elevated the mRNA levels of other syndecans. When *SDC2* was knocked down, *SDC3* and *SDC4* were significantly increased. *SDC3* knockdown resulted in upregulation of *SDC4*, and *SDC4* knockdown elevated *SDC2* and *SDC3*. Interestingly, siRNA silencing of *SDC2* or *SDC3* (but not *SDC4*) increased *FBLN4* and *LTBP4* mRNA expression (Figure 5H). The mRNA expression levels of *tropoelastin* and *ELN* in all transfected cells remained similar to the scrambled siRNA control (Figure 5H).

Following siRNA gene silencing of *SDC2*, *3*, or *4*, NSF binding was tested to FBLN4 and LTBP4 isoforms, as well as to tropoelastin and pFN controls (Figure 5I). Knockdown of *SDC2* or *SDC3* abolished the interaction of NSF with FBLN4, whereas only *SDC3* knockdown abolished the interaction with LTBP4L or LTBP4S. On the contrary, the knockdown of *SDC4* did not alter NSF interaction with either FBLN4 or LTBP4. Binding to tropoelastin or pFN was not negatively affected by any of the SDC knockdowns and, in some cases, even increased cell binding.

To extend the study to elastogenic SMC, we applied the same siRNA knockdown strategy to inhibit the mRNA expression of *SDC2-4* in umbilical arterial smooth muscle cells (Figure S1B,C). Consistent with the data obtained with NSF, single *SDC* siRNA knockdowns in these SMC were specific and resulted in a higher mRNA expression of other SDCs (Figure S1B). Also, the mRNA expression levels of FBLN4 and LTBP4 increased when *SDC2* or *SDC3* were knocked down. Similar to the effect of knocking down *SDCs* in skin fibroblasts, SMC adhesion to FBLN4 was significantly reduced when *SDC2* or *SDC3* were siRNA-silenced, and only the *SDC3* siRNA knockdown significantly decreased SMC binding to both LTBP4 isoforms (Figure S1C). Knockdown of SDC4 did not reduce SMC interaction with either FBLN4 or LTBP4 isoforms.

3.6 | FBLN4 interacts with SDC2 and SDC3 ectodomains, whereas LTBP4 only interacts with the SDC3 ectodomain

Each SDC contains an N-terminal ectodomain that carries several heparan sulfate chains either at the distal end (SDC2 and 4) or heparan sulfate and chondroitin sulfate at the distal and proximal ends, respectively (SDC3).[49] Here, we analyzed if FBLN4 and LTBP4 directly interact with the relevant SDC ectodomains. Therefore, we produced recombinant ectodomains of each SDC (SDC-ED) by human 293-EBNA cells to ensure proper post-translational modifications in the secretory pathway, including heparan sulfate synthesis. The constructs included N-terminal hexahistidine tags and C-terminal FLAG tags, omitting the transmembrane and cytosolic domains (Figure 6A). The proteins were secreted into the culture medium at low concentrations, insufficient for chromatographic protein purification. However, ELISA analyses of the conditioned medium clearly showed the presence of the recombinant SDC-ED in the culture medium in similar relative concentrations (Figure 6B). This

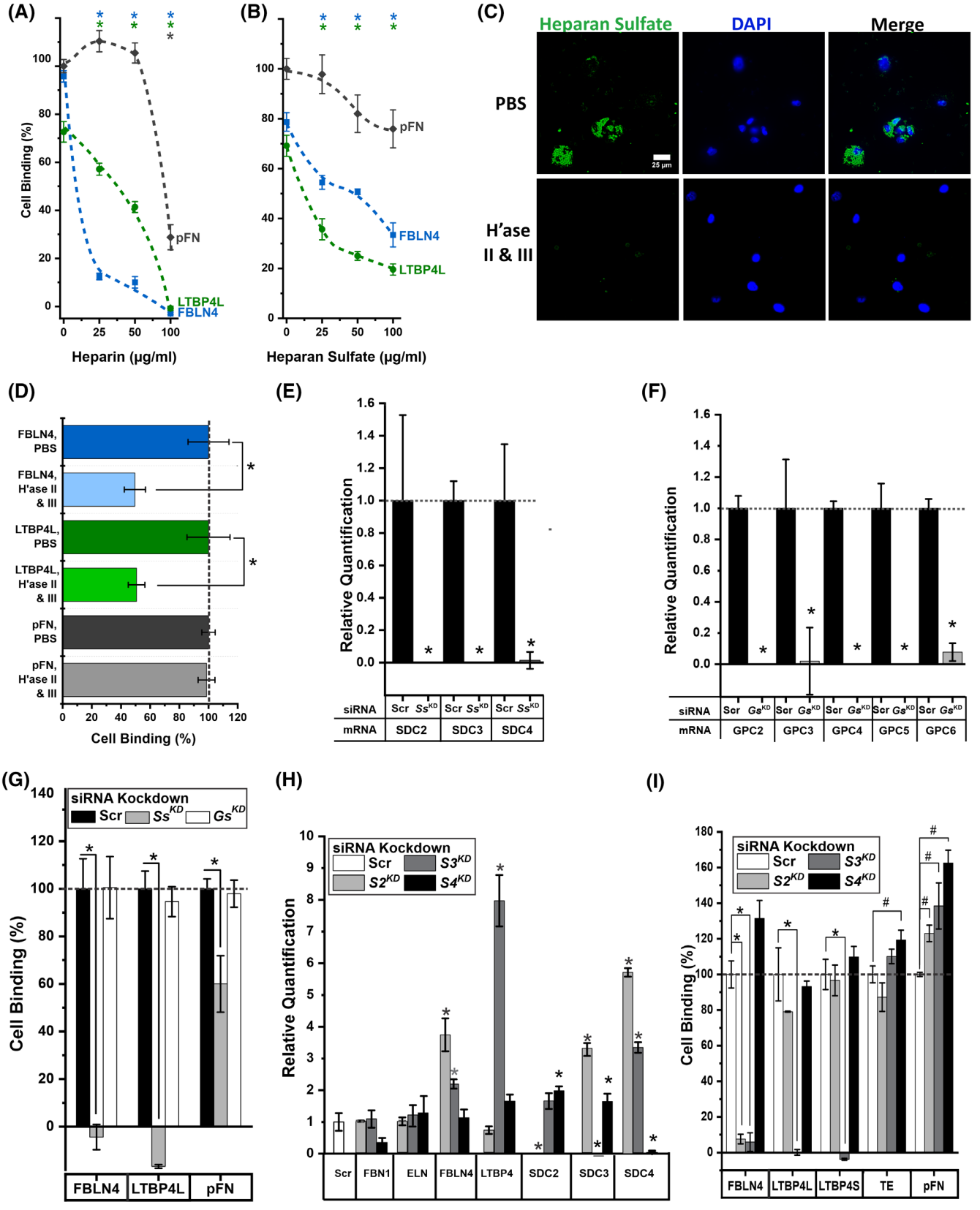

allowed us to perform solid phase binding assays with immobilized FBLN4 and LTBP4 and serially diluted conditioned media, containing the recombinant SDC-EDs in the soluble phase, specifically detectable by an anti-FLAG antibody. Concentrated conditioned medium from non-transfected cells served as a negative control. Representative solid phase binding assays using soluble SDC-EDs and immobilized FBLN4, LTBP4L, LTBP4S,

FIGURE 5 Heparan sulfate and syndecans mediate cell interaction with FBLN4 and LTBP4. (A, B) Interaction of NSF with FBLN4, LTBP4L, and pFN as a control was analyzed in the presence of 0–100 μg/mL heparin (A) and heparan sulfate (B). Shown is one representative experiment with 4 replicates of 3 experiments total. (C) Skin fibroblasts were treated with Heparinases II and III (H'ase II & III) in suspension, and then stained on a glass slide with an anti-heparan sulfate antibody (green signal). The cell nuclei were counterstained by DAPI. The scale bar represents 25 μm. (D) H'ase II & III-treated fibroblasts were used in crystal violet cell binding assays to analyze their interactions with FBLN4 and LTBP4L, and with pFN as control. Error bars represent the standard deviation of replicates of one representative experiment (3 experiments total). Statistical analyses were performed using the student *t*-test. (E) Real-time qPCR quantification of *SDC2*, *SDC3*, and *SDC4* mRNA levels in NSF that were transfected with either scrambled siRNA (Scr) or a pool of specific siRNA designed to knock down *SDC2*, *SDC3*, and *SDC4* (Ss^{KD}). (F) Similarly, the mRNA expression levels of *GPC2-6* were relatively quantified after transfection with either scrambled siRNA (Scr) or a specific siRNA pool designed to knock down *GPC2-6* (Gs^{KD}). Data in (E) and (F) are represented as means of ΔΔCT ($n = 3$). GAPDH and RPL13A were used as housekeeping genes, and the mRNA level in the knockdown sample was compared relative to its expression in the scrambled siRNA control. (G) NSF transfected with scrambled siRNA or with specific siRNA pools for *SDC2*, *SDC3*, and *SDC4* or *GPC2-6* were used to analyze interactions with FBLN4 and LTBP4L 3 d after transfection ($n = 3$). Error bars represent the standard deviation of 4 replicates of one representative experiment (3 experiments total). (H) Relative quantification of mRNA levels by real-time qPCR for *tropoelastin*, *ELN*, *FBLN4*, *LTBP4L*, and *SDC2-4* in human skin fibroblasts transfected with either scrambled siRNA (Scr) or siRNA specific for SDC2, SDC3, or SDC4. GAPDH and RPL13A mRNA were used as endogenous references, and each mRNA was compared relative to its expression in the scrambled control (set to 1). Data in (H) are represented as means of ΔΔCT ($n = 3$). (I) Human skin fibroblast binding to FBLN4, LTBP4L, LTBP4S, tropoelastin, and pFN was assessed at 3 d after siRNA transfection targeting SDC2, SDC3, and SDC4 ($n = 5$). * indicate significant decreases, whereas # indicate significant increases in cell adhesion compared to the scrambled controls. Statistical analyses were performed using two-way ANOVA with *p*-values ≤.05 taken as statistically significant.

pFN, and BSA are shown in Figure 6C–G. pFN was used as a positive control, and BSA as a negative control for all interaction assays with SDC-EDs. FBLN4 showed strong binding to both SDC2-ED and SDC3-ED, whereas both LTBP4L and LTBP4S interacted only with SDC3-ED. As expected from other studies, pFN interacted with SDC2-ED and SDC4-ED but not with SDC-ED3.[50–52] None of the recombinant SDC-EDs interacted with BSA. To complement these data with another protein interaction assay, we used surface plasmon resonance (SPR) spectroscopy (Figure 6H). FBLN4, LTBP4L, and LTBP4S were immobilized on sensor chips and allowed to interact with soluble SDCs present in the 20-fold concentrated conditioned media. Similar to the findings from the solid phase assays, FBLN4 showed strong interactions with SDC2 and SDC3. The dissociation rate k_d was $4.1 \pm 0.9 \times 10^{-4}\,s^{-1}$ for SDC2 and $8.2 \pm 1.3 \times 10^{-4}\,s^{-1}$ for SDC3. LTBP4L and LTBP4S showed stable interactions only with SDC3 with k_d values of $5.5 \pm 0.5 \times 10^{-5}\,s^{-1}$ for LTBP4L and $6.3 \pm 1.1 \times 10^{-5}\,s^{-1}$ for LTBP4S. We could not analyze the association rate k_a or the dissociation constant K_D, because the concentrations of the SDCs in the conditioned media could not be determined. SDC4 did not interact with FBLN4 or the LTBP4 isoforms.

To further corroborate that FBLN4 and LTBP4 cell interactions are mediated through the identified SDC-EDs, we implemented a cell binding inhibition strategy (Figure 6I). 20-fold concentrated conditioned media containing recombinant SDC-EDs were preincubated with the immobilized FBLN4 or the LTBP4 isoforms prior to the cell binding assay to compete for their binding to NSF. Additionally, we included pFN as a control. Consistent with the results of the solid phase binding assay and the SPR spectroscopy, conditioned media containing SDC2-ED or SDC3-ED strongly inhibited cell interaction with FBLN4, whereas only SDC3-ED-containing medium inhibited cell interaction with LTBP4L or LTBP4S. NSF binding to pFN was not inhibited by any SDC-ED.

In summary, these data demonstrate direct interactions of FBLN4 with SDC2-ED and SDC3-ED and of both LTBP4 isoforms with SDC3-ED. The results are consistent with and confirm the data obtained by the siRNA knockdown approach.

3.7 | FBLN4 and LTBP4 stimulate focal adhesion formation

It is well known that cell adhesion to ECM proteins promotes focal adhesion (FA) formation, which in turn can reinforce matrix assembly, for example, for cell interactions with fibronectin.[52,53] To investigate if FBLN4 and LTBP4 cell interactions enhance FA formation, phosphorylated focal adhesion kinase (pFAK) was evaluated as a proxy readout of skin fibroblasts cultured 24 h on immobilized pFN, FBLN4, and LTBP4L. Western blotting of cell lysates revealed a significant upregulation of pFAK when cells were cultured on pFN, FBLN4, or LTBP4L, compared to the buffer control (Figure 7A,B). pFAK immunostaining

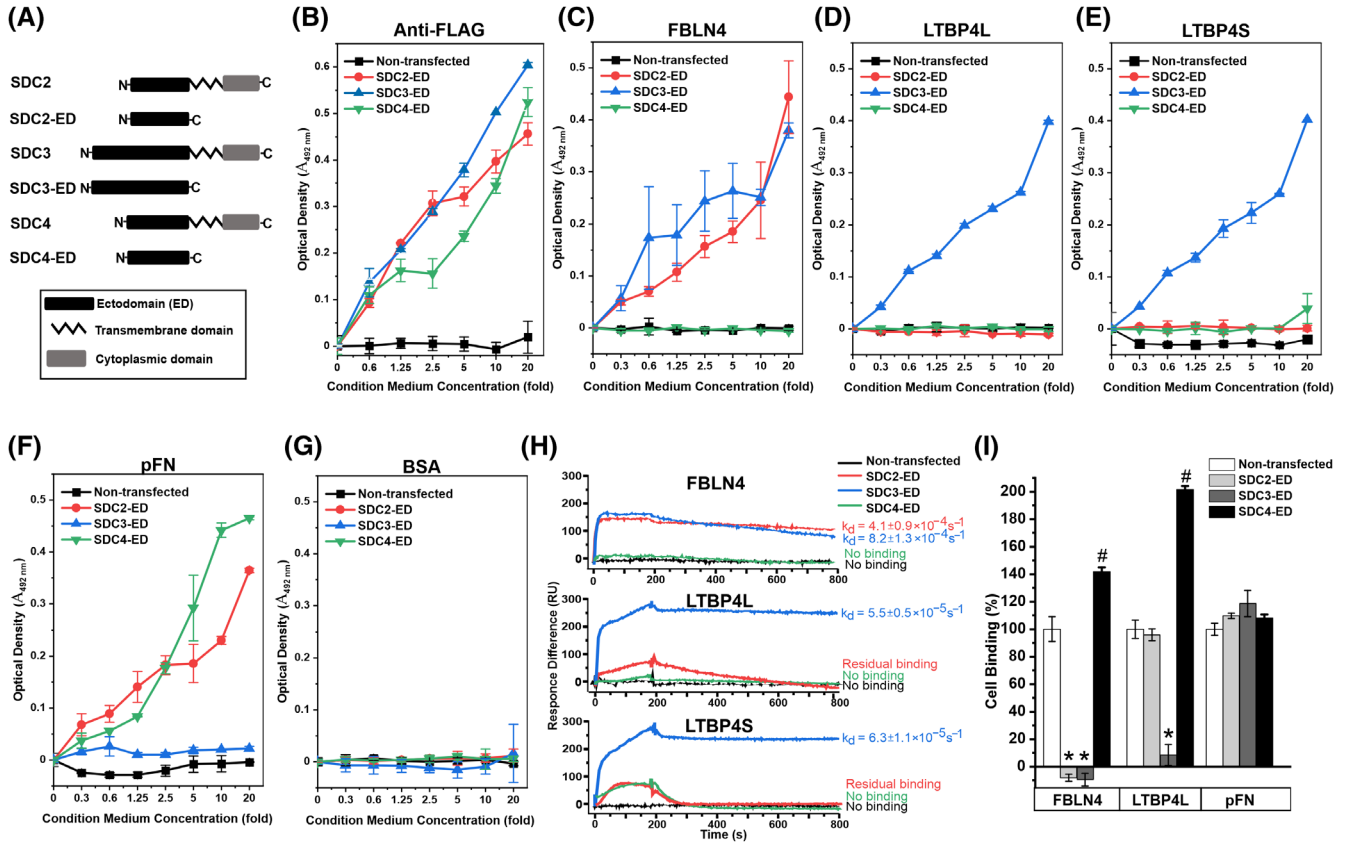

FIGURE 6 Syndecans interact directly with FBLN4 and LTBP4 isoforms. (A) Schematic presentation of the domain arrangement of full-length syndecan proteins (SDC2-4) and the recombinant syndecan ectodomain constructs (SDC2-ED, SDC3-ED, SDC4-ED), which were FLAG-tagged at the N-terminal end after the signal peptide. (B) The presence of FLAG-tagged SDC2-ED, SDC3-ED, and SDC4-ED in the conditioned cell culture media was confirmed by ELISA. Conditioned media from HEK 293 EBNA cells that were either non-transfected or transfected with the recombinant SDC-ED plasmids were concentrated up to 20-fold, coated in quadruplicates into 96-well plates, and analyzed using an anti-FLAG-tag antibody. (C–G) Representative solid phase binding assays with immobilized FBLN4 (C), LTBP4L (D), LTBP4S (E), pFN (F), and BSA (G) and serial dilutions (0–20-fold) of conditioned media from HEK 293 EBNA cells either non-transfected or transfected with the SDC-ED expressing plasmids. (H) Surface plasmon resonance spectroscopy of FBLN4, LTBP4L, and LTBP4S immobilized on the sensor and 20-fold concentrated conditioned media containing recombinant SDC-EDs as soluble analytes as indicated. 20-fold concentrated conditioned medium from non-transfected cells served as control. Dissociation rates k_d are shown. Association rates k_a and dissociation constants K_D could not be determined because of the unknown concentrations of SDC-EDs in the medium. (I) Inhibition assay of fibroblasts binding to FBLN4, LTBP4L, LTBP4S, and pFN in the presence of 20-fold concentrated conditioned media as described above. * Indicates significant decreases, whereas # indicates significant increases in NSF adhesion. Statistical analyses were performed using two-way ANOVA with p-values ≤.05 taken as statistically significant.

showed significantly higher numbers and total amounts of FAs when fibroblasts were seeded on pFN, FBLN4, or LTBP4L-coated surfaces (Figure 7C–E). In summary, these results show that FBLN4 and LTBP4L promote FA formation and activation.

3.8 | FBLN4 and LTBP4 cell interactions induce cell contraction

The stress fiber and FA promoting property of FBLN4 and LTBP4 (Figure 1E,F) suggested that these proteins can induce cell contraction and thereby exert tension on the surrounding matrix, which may be necessary for elastic fiber formation. To test the role of FBLN4 and LTBP4 on cell contractility, skin fibroblasts were cultured in 3-dimensional collagen type I gels, containing either 10 μg/mL FBLN4, LTBP4L, or the buffer control (TBS, Ca^{2+}) using gel contraction as a readout. We confirmed that the fibroblasts were differentiated into contractile myofibroblasts by immunostaining with αSMA antibodies (Figure S2). Addition of FBLN4 or LTBP4L significantly increased contraction of the fibroblast-cellularized collagen gels at all analyzed time points (Figures 7G,H and S2). The results confirm that both FBLN4 and LTBP4 induce cell contraction.

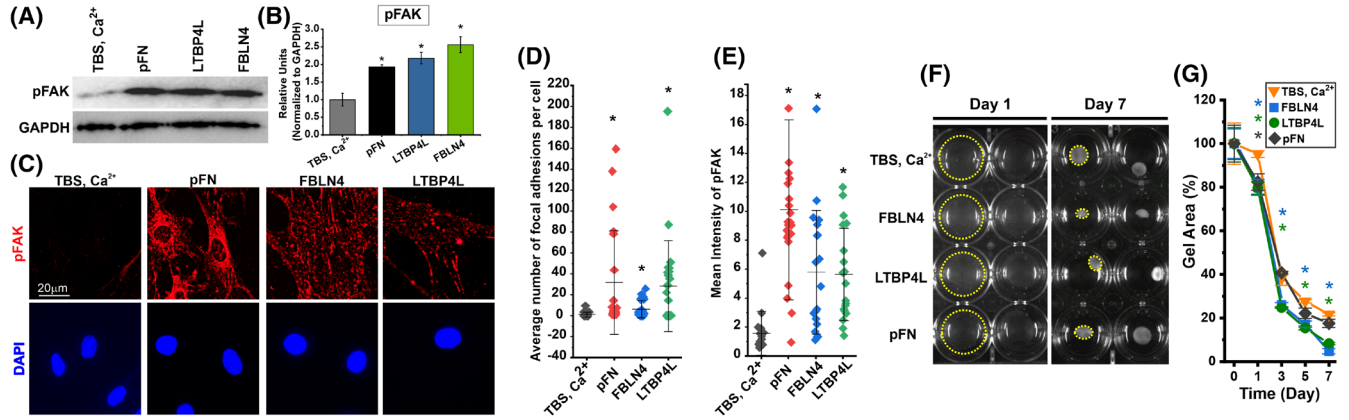

FIGURE 7 FBLN4 and LTBP4 cell interactions promote focal adhesion formation and cell contraction. (A) NSF were kept in culture wells coated with FBLN4, LTBP4L, pFN for 24 h. TBS, 2 mM Ca^{2+} was used as a buffer control. Cell lysates were prepared and used for immunoblotting with an anti-pFAK antibody. GAPDH was utilized as an internal control. (B) Quantification of pFAK levels analyzed by Western blotting shown in A ($n = 3$). The values are presented as relative ratios to the buffer control after normalizing pFAK signals to the corresponding GAPDH signals for each sample. (C) IF staining of pFAK (red) was performed 24 h after culturing skin fibroblasts in 8-well chamber slides coated with either FBLN4, LTBP4L, pFN, or TBS, 2 mM Ca^{2+} as buffer control. DAPI (blue) was used for nuclei counterstaining. The scale bar represents 20 μm for all images. (D, E) Quantification of the red pFAK signals in (C) in terms of average number of focal adhesions per cell (D) and total mean intensity of pFAK (E). Statistical analyses in (D, E) were performed using the unpaired Student's two-tailed t-test. (F) Skin fibroblasts were subjected to a 3D-collagen type I gel contraction assay to test the effect of FBLN4 and LTBP4L on cell contractility. Images of floating non-cellularized and cellularized collagen gels were recorded at days 0, 1, 3, 5, and 7. Representative images are shown for days 1 and 7. The comparison with non-cellularized gels is shown in Figure S2. TBS, 2 mM Ca^{2+} was used as a buffer control. Some collagen gels are circled with a yellow outline for clarity. (G) The collagen gel areas in (F) were quantified at the indicated time points and are presented in percentage relative to the gel areas at the start time point. The significant reduction in the gel area is indicated by color-coded asterisks on top of the graph matching the color code of the corresponding protein. Error bars represent standard deviation of 2 replicates of one representative experiment (3 experiments total). Statistical analyses were performed using two-way ANOVA. * Indicates statistical significance with p-values ≤.05.

3.9 | FBLN4 and LTBP4 cell interactions elevate Erk1/2 protein expression and RhoA activation

Since we determined that FBLN4 and LTBP4 cell interactions affect FA formation and trigger cell contraction, we continued to analyze the signaling pathway involved in these cellular mechanisms. It is known that Rho family GTPases are regulators of actin filament remodeling leading to cell contraction.[54–56] RhoA regulates actin filament assembly and actin polymerization.[57,58] ECM proteins and growth factors stimulate FA formation and new actin stress fibers via RhoA signaling.[56,59] In addition, activation of Erk1/2 also induces cell contraction by promoting a RhoA-mediated increase in actin stress fiber formation.[60–62] Therefore, to determine the pathway underlying FBLN4- and LTBP4-induced FA formation and cell contraction, we analyzed Erk1/2 and RhoA levels and activation status in NSF seeded on FBLN4 and LTBP4L for 24 h by immunostaining (Figure 8A). The signal intensities of both total and phosphorylated Erk1/2 (tErk1/2 and pErk1/2, respectively) were significantly increased in NSF cells seeded on immobilized FBLN4, LTBP4L, or the positive pFN control (Figure 8B,C). Additionally, the cells displayed a moderate increase in total RhoA levels, together with a marked elevation in active RhoA in all protein-coated conditions (Figure 8D,E). These results suggest that cell interactions with FBLN4 and LTBP4 promote focal adhesion formation and cell contraction through Erk1/2 and RhoA activation.

3.10 | siRNA knockdown of syndecans results in compromised elastic fibers

The functional consequence of cell interactions with FBLN4 and LTBP4 on elastic fiber formation was tested through immunostaining of tropoelastin. NSF cultured on FBLN4 and LTBP4L-coated surfaces showed significantly increased elastic fiber formation as compared to non-treated conditions (Figure 9A,B). pFN was used as a positive control in these experiments. The interaction of either FBLN4 or LTBP4L with cells did not alter *ELN* gene expression, nor did it affect the expression of *SDC2* and *SDC3* (Figure S3). The data suggest that the increased elastic fiber formation in the presence of FBLN4

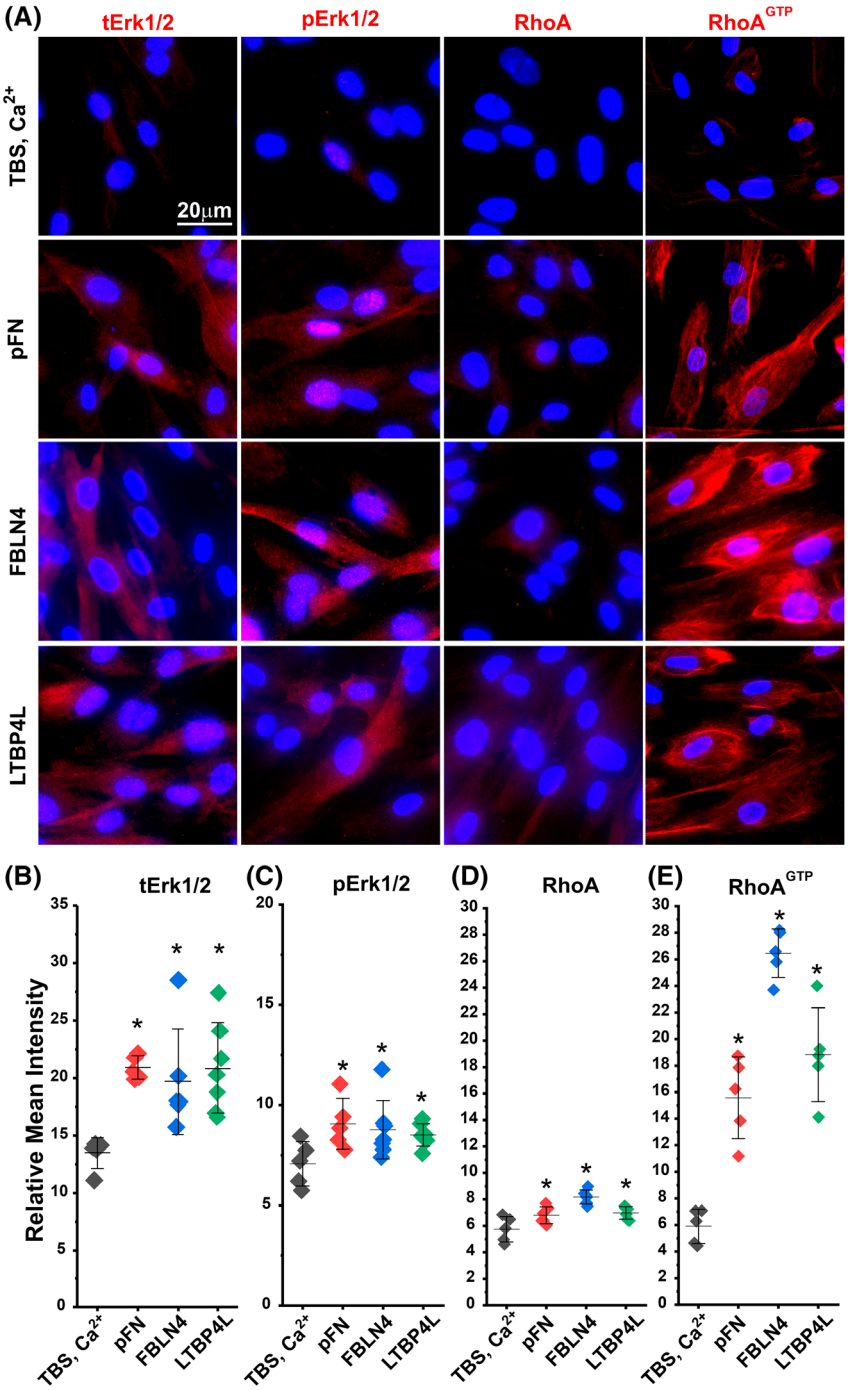

FIGURE 8 FBLN4 and LTBP4 cell interactions elevate Erk1/2 and RhoA activation. (A) Immunofluorescence analyses of tERK1/2, pErk1/2, RhoA, and $RhoA^{GTP}$ (red signals) in NSF cultured for 24 h on FBLN4-, LTBP4L-, or pFN-coated wells. TBS, 2 mM Ca^{2+} was used as a buffer control. DAPI (blue) was used for nuclei counterstaining. The scale bar represents 20 μm for all images. (B–E) The signal intensity of the IF staining presented in (A) was quantified as relative mean intensity per cell. The signals for the NSF seeded on TBS, 2 mM Ca^{2+} were set to 1. Statistical analyses were performed using the unpaired Student's two-tailed *t*-test. Each data point in the quantification graphs represents an individual cell. Error bars represent standard deviation of cells from 2 replicates of one representative experiment (3 experiments total). * Indicates statistical significance with *p*-values ≤.05.

and LTBP4 is mediated through enhanced tropoelastin assembly via elevated cell contraction. We assessed the consequences of *SDC*-specific siRNA silencing on elastic fiber assembly in immunolabeled NSF cultures (Figure 9C,D). Silencing *SDC2* and *SDC3* expression resulted in severely compromised and reduced elastic fiber assembly/deposition in the ECM. These results demonstrate that SDC2 and SDC3 are pivotal in the assembly/

deposition of elastic fibers, mediated by FBLN4 and LTBP4 cell interactions.

3.11 | FBLN4 and LTBP4 promote elastogenesis through focal adhesion kinase, Erk1/2, and RhoA-mediated cell contraction

To test and validate whether the FBLN4- and LTBP4-mediated elastogenesis operates through FAK, ERK1/2, and RhoA signaling, we seeded NSF on FBLN4- and LTBP4L-coated surfaces and inhibited the target molecules pharmacologically using cognate inhibitors for FAK (PF573228), ERK1/2 (SCH772984), and RhoA (CCG-1423). NSF was treated with these inhibitors for 5 d and analyzed for tropoelastin assembly using immunofluorescence staining (Figure 9E,F). The inhibition of FAK, ERK, and RhoA all significantly reduced tropoelastin assembly and elastic fiber formation under FBLN4- and LTBP4L-coated conditions independent of the protein coating concentrations of 10 or 25 μg/mL. Notably, the mRNA levels of elastin remained unaffected under inhibitor-treated conditions (Figure S4A–D). These results demonstrate that the cell contraction regulators FAK, ERK, and RhoA are essential for elastic fiber formation.

To further validate that cell interactions of FBLN4 and LTBP4L with SDC2 and SDC3 regulate pFAK, ERK, and RhoA signaling during elastic fiber formation, we analyzed these intracellular pathways following siRNA knockdown of SDC2 and SDC3 in fibroblasts seeded on FBLN4-r LTBP4L-immobilized surfaces. Cells transfected with the scrambled siRNA control and seeded on FBLN4 or LTBP4L showed a significant increase in pERK, pFAK, and $RhoA^{GTP}$ levels compared to cells seeded on the buffer control-treated surface (Figure 10A,B). Knockdown of SDC2 or SDC3 resulted in a significant reduction in pERK, pFAK, and $RhoA^{GTP}$ levels compared to the scrambled controls (Figure 10A,B). These results establish that FBLN4 and LTBP4L-mediated interactions with SDC2 and SDC3 facilitate pERK, pFAK, and $RhoA^{GTP}$ signaling pathways.

3.12 | FBLN4- and LTBP4-mediated cell contraction is critical for elastic fiber formation

Since we identified that FBLN4- and LTBP4-mediated cell interactions via SDC2 and SDC3 promote cell contraction and elastogenesis, we next evaluated the direct role of cell contraction in elastic fiber formation. We employed the well-established cell-permeable myosin II inhibitor blebbistatin, which inhibits non-muscle myosin II ATPases,[63] to inhibit contraction of NSF seeded in collagen type I gels. As expected, we observed significantly less contraction of the fibroblast-containing gels treated with active blebbistatin compared to the inactive blebbistatin control (Figure 11A,B). In addition, a clear reduction in stress fiber formation also marked compromised cell contractility in the presence of active blebbistatin (Figure 11C,D). No significant changes in the expression of ELN, FBLN4, or LTBP4 genes were observed under the inhibitor-treated conditions (Figure S4E–G). Inhibition of cell contraction by blebbistatin resulted in severely impaired elastic fiber formation and inhibition of FBLN4 and LTBP4 assembly/deposition, but not FN assembly (Figure 11C–G). The results show that cell contraction is indispensable for the assembly of these key elastogenic proteins.

4 | DISCUSSION

Elastogenesis is a developmental process of elastic fiber formation in large blood vessels, lungs, skin, and other elastic tissues with fetal onset until late adolescence.[1,64] The formation of a complex elastic fiber network is vital for the function of elastic tissues. The focus of this study was to explore and functionally characterize cell interactions of two elastic fiber-associated proteins, FBLN4 and LTBP4, in the context of elastogenesis. Previous studies have demonstrated that FBLN4 and LTBP4, which both lack typical Arg-Gly-Asp integrin binding sites, interact with elastogenic cells.[32,33] However, the mechanisms of these interactions are not well understood. The presented data reveal essential insight into FBLN4 and LTBP4 cell interactions, identify the respective cell receptors, and emphasize the significance of these cell interactions in elastogenesis.

We previously demonstrated that FBLN4 multimerizes under physiological conditions.[32] Here, we determined with monomeric, dimeric, and multimeric FBLN4 that multimerization is a prerequisite and essential for the protein to interact with skin fibroblasts and vascular smooth muscle cells. We also demonstrated earlier that FBLN4 multimers interacted much stronger with heparin than dimers and monomers.[32] Those findings strongly suggested that cells may interact with FBLN4 multimers through heparan sulfate glycosaminoglycans, which are similar to heparin, on the cell surface. Interaction with cell surface heparan sulfate may require a higher avidity of low-affinity binding sites present in monomers, which is typically achieved by multimerization.[65] In addition, Kumra et al. demonstrated that only FBLN4 multimers efficiently interacted with LTBP4

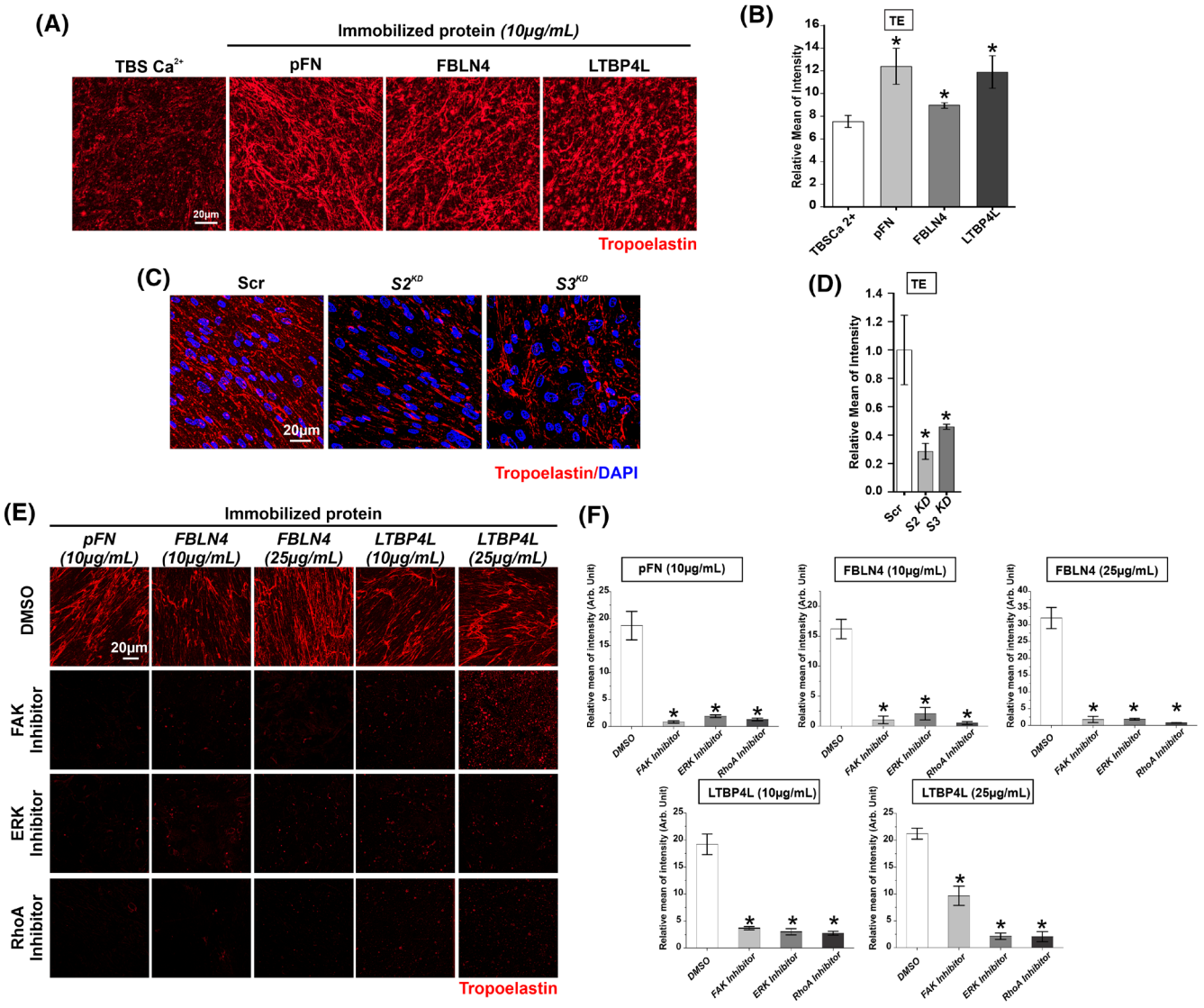

FIGURE 9 Interaction of FBLN4 and LTBP4 with syndecan-2 and -3 is essential for elastogenesis. (A) Representative images of tropoelastin immunostaining of NSF seeded for 5 d on non-coated versus protein immobilized (10 μg/mL) conditions as indicated. (B) Quantification of the mean tropoelastin signal intensities from the data in (A). The experiment was performed 3 times with 3 replicates each. Error bars represent standard deviations using 6–10 images of one representative experiment. (C) Representative immunofluorescence images after siRNA knockdown of syndecan-2 and -3 ($S2^{KD}$, $S3^{KD}$) of tropoelastin deposited by NSF within 5 d. (D) Quantification of the tropoelastin staining in (C) relative to the scrambled siRNA control (Scr) set to 1. The experiment was performed 3 times with 4 replicates each. Error bars represent the standard deviations of one representative experiment. (E) tropoelastin immunostaining of NSF cultivated on immobilized proteins (10 μg/mL or 25 μg/mL) in medium containing 0.1% DMSO with or without inhibitors as indicated. (F) Quantification of the tropoelastin signal intensities shown in (E). The experiment was performed 3 times with 3 replicates each. Error bars represent standard deviations using 5–7 images of one representative experiment. Statistical analyses were performed using one-way (B, F) or two-way (D) ANOVA. Scale bar on images represents 50 μm (A) or 20 μm (C, E). * Indicates statistical significance with p-values ≤.05.

and with fibronectin.[30] In turn, Kantola et al. showed that LTBP4 also interacts with heparin, suggesting that it interacts with cell surface-located heparan sulfate.[33] The binding of FBLN4 and LTBP4 to heparan sulfate moieties may serve to bring these proteins in physical proximity to enable the previously described chaperone function of FBLN4 required to extend the compact LTBP4, which enables interactions with microfibrils.[30] Previously, FBLN4 multimerization was attributed to a region spanning cbEGF2-5 and a region encompassing cbEGF6 and the unique C-terminal domain.[30] In the present study, we mapped the multimerization domains more precisely to cbEGF4-5 and the C-terminal domain. Since these regions are located relatively close to each other, only separated by cbEGF6, it is possible that they represent part of a contiguous multimerization domain spanning this region, rather than two separated functional domains. Presumably, a contiguous site at the

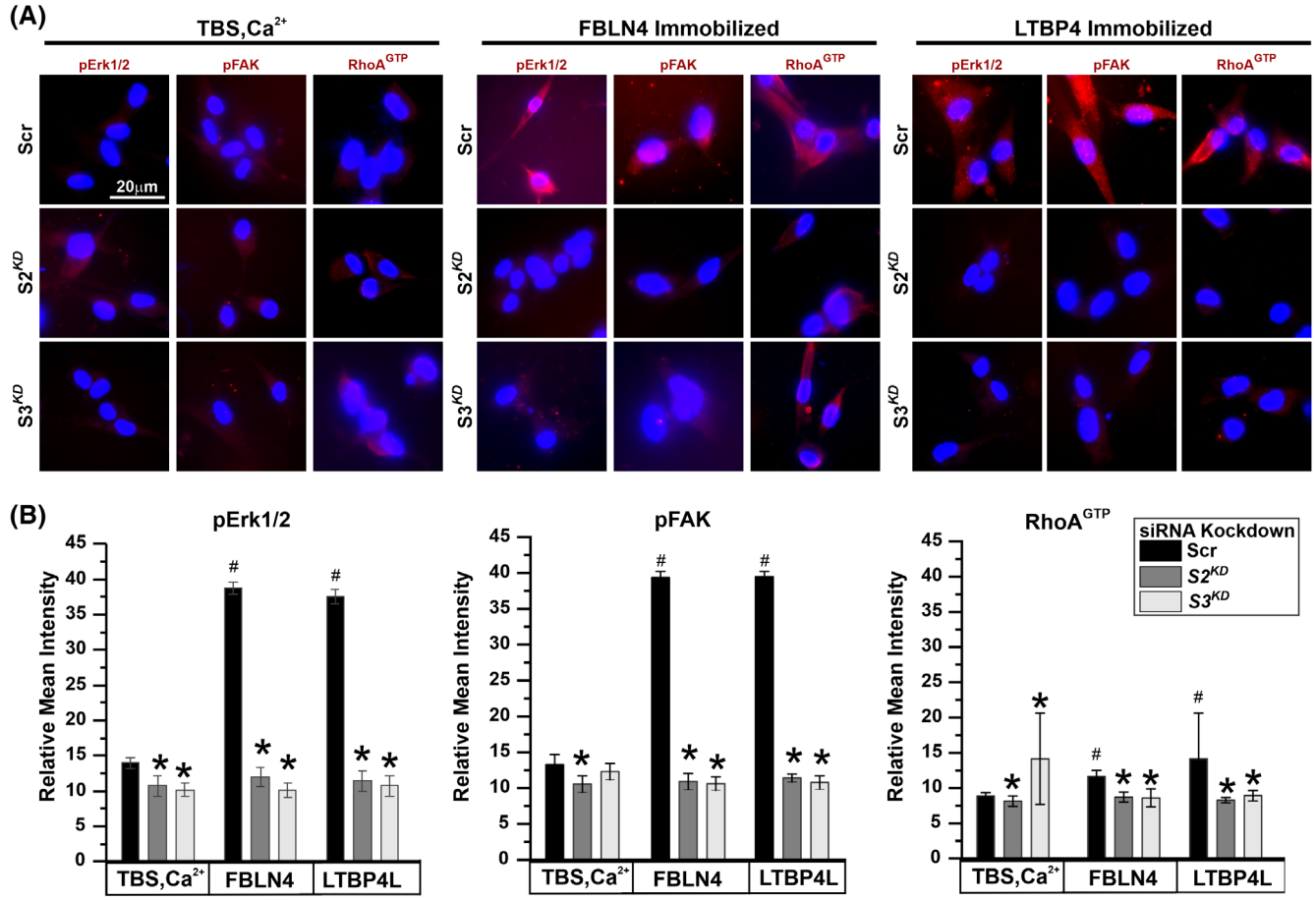

FIGURE 10 Knockdown of SDC2 and SDC3 impairs pFAK, Erk1/2, and RhoA activation. (A) Representative images of pErk1/2, pFAK, and $RhoA^{GTP}$ immunostaining (red signals) after siRNA knockdown of SDC2 and SDC3 ($S2^{KD}$, $S3^{KD}$) in NSF cultured for 24 h on either FBLN4, LTBP4L, or pFN-coated wells. TBS, 2 mM Ca^{2+} was used as a buffer control. DAPI (blue) was used for nuclei counterstaining. The scale bar presents 20 μm for all images. (B) Quantification of the pErk1/2, pFAK, and $RhoA^{GTP}$ staining intensities in (A). The experiments were repeated 3 times with 2 replicates each. Error bars represent the standard deviations of one representative experiment. * Indicates significance ($p \leq .05$) between comparisons of scrambled controls versus SDC knockdowns within a coating condition. # Indicates significance ($p \leq .05$) between non-coated versus protein-coated conditions of the scrambled controls. Statistical analyses were performed using the unpaired Student's two-tailed *t*-test.

C-terminal region of FBLN4 would only be able to mediate multimerization when the protein is completely synthesized and translocated into the endoplasmic reticulum. However, the precise subcellular localization for FBLN4 multimerization either in the endoplasmic reticulum, the Golgi apparatus, or on the cell surface after secretion remains to be established.

To refine the mapping of the cell interaction sites on FBLN4, we examined multiple deletion mutants that localized the cell binding properties to two regions: cbEGF2-3 and the C-terminal domain. We have previously predicted these sites based on clusters of basic amino acid residues in cbEGF3 and the C-terminal domain that rendered these sites ideal for interaction with negatively charged heparan sulfate.[32] Interestingly, the cell binding site in the C-terminal domain overlaps with the multimerization domain, and deletion mutants containing cbEGF2-3 and the C-terminal domain self-interact and bind to LTBP4 and fibronectin,[30] suggesting a regulatory function of FBLN4 cell interaction in elastogenic mechanisms. For LTBP4, one cell binding site was previously mapped by Kantola et al. to a region spanning TB2-TB3 close to the C terminus using full-length recombinant LTBP4S and several smaller fragments.[33] Here, we show that LTBP4S and LTBP4L bind similarly to elastogenic cells, which is consistent with these published data. This is further supported by our analysis, which shows the presence of basic stretches of amino acid residues in the two linker sequences adjacent to TB2 that overlap with the mapped cell interaction site (Figure 3). Importantly, TB2 represents the domain that covalently binds the small latent TGF-β complex.[66,67] In this context, it is possible that cell binding adjacent to this complex may position it on the cell surface for subsequent TGF-β activation. Analyzing cell interaction in

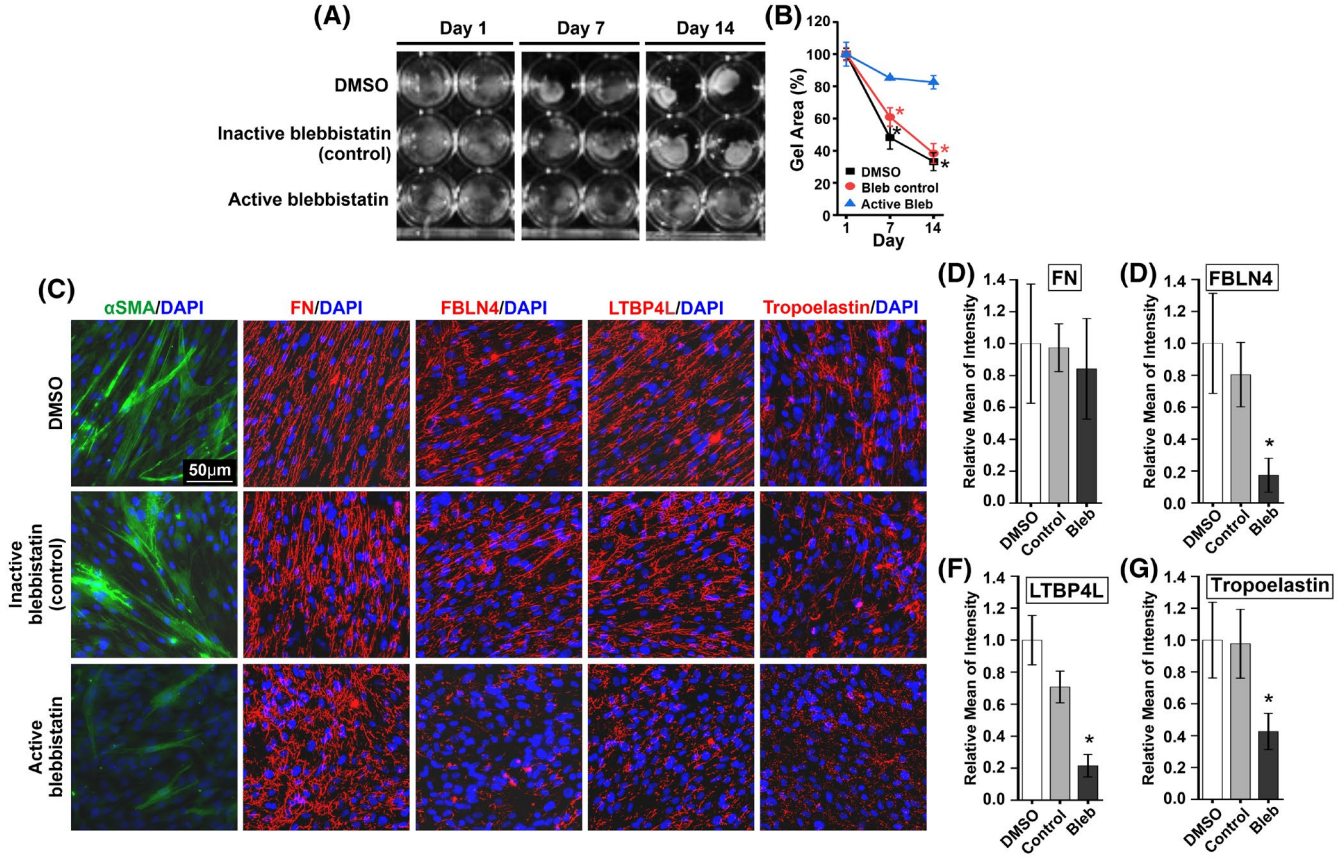

FIGURE 11 FBLN4- and LTBP4L-induced cell contraction mediated through syndecan-2 and -3 is required for elastogenesis. (A) NSF were subjected to a 3D-collagen type I gel contraction assay in the presence of 50 μM active and inactive blebbistatin to inhibit cell contraction. Images of floating collagen gels were recorded between 1 and 14 d. (B) The collagen gel areas from (A) were quantified and are presented relative to the gel areas at 1 d. A significant reduction in gel areas relative to the DMSO control is indicated by color-coded asterisks. The experiment was performed 2 times with 3 replicates. One representative experiment is shown with standard deviations of the triplicates. (C) Representative immunofluorescence images of αSMA, FN, FBLN4, LTBP4, and tropoelastin deposited by NSF over 7 d cultivated in 0.1% DMSO alone or containing active and inactive blebbistatin as indicated. The scale bar presents 50 μm for all images. (D–G) Quantification of the FN, FBLN4, LTBP4, and tropoelastin staining intensities in (C). The signals from the DMSO-only controls were set to 1. The experiments were repeated 3 times with 4 replicates each. Error bars represent the standard deviations of one representative experiment. Statistical analyses were performed using two-way ANOVA. * Indicates statistical significance with p-values ≤.05.

the present study with recombinant fragments of LTBP4S and LTBP4L further revealed the presence of a novel additional interaction site in the N-terminal half of both LTBP4 isoforms. This is supported by the presence of additional basic regions located close to the N-terminus of LTBP4S and LTBP4L and from TB1 to cbEGF2 (Figure 3). Both are candidate regions for cell interactions with the N-terminal halves. We have previously suggested that LTBP4 is held in a compact conformation through N- to C-terminal self-interactions.[30] This compact conformation can be extended by interaction with FBLN4, a mechanism that, in turn, promotes elastic fiber formation. Cell interaction with the N- and C-terminal regions of LTBP4 may, hence, play a regulatory role in elastogenic fiber formation. For example, it could position compact LTBP4 close to cell-bound FBLN4 to promote interaction and LTBP4 extension.

Through a series of biochemical and cell biological experiments, we identified SDC2 and SDC3 as the cell surface receptors for FBLN4 and SDC3 as the LTBP4 receptor. siRNA knockdown experiments of SDCs, cell binding experiments under heparin/heparan sulfate competition or after degradation of cell surface heparan sulfate, and direct binding assays of FBLN4 and LTBP4 with SDC2 and SDC3 all fully supported these results. SDCs can form homotypic and heterotypic dimers to function as cell receptors.[38] In this light, it is possible that FBLN4 interacts with a heterodimer of SDC2 and SDC3 because knocking down one of them led to the loss of cell interactions. It is not clear if LTBP4 binds to cells through monomeric or homodimeric SDC3. Since LTBP4 requires FBLN4 as a chaperone to trigger an extended confirmation,[30] a defined interaction of FBLN4 with an SDC2 and SDC3 heterodimer may facilitate transient interactions of FBLN4 with LTBP4 bound to

a separate SDC3 monomer or homodimer. This scenario is more likely than a simultaneous interaction of FBLN4 and LTBP4 with the same SDC2/SDC3 heterodimer because it only requires a brief contact of FBLN4 to initiate the extended conformation of LTBP4.[30]

We identified that cells, upon interaction with FBLN4 and LTBP4, increased cell contraction and elastic fiber formation. The elevated levels of elastic fibers induced by FBLN4 and LTBP4 were primarily due to enhanced tropoelastin assembly, as there were no significant changes in tropoelastin mRNA levels. Our data are consistent with the interpretation that FBLN4 and LTBP4 interact with SDC2 and/or SDC3 to transduce signals from the ECM through their transmembrane and cytoplasmic domains, facilitating the assembly of tropoelastin to form elastic fibers. Our experiments show that cell interaction with FBLN4 and with LTBP4 enhanced stress fiber formation, suggesting that these proteins can instruct cells to contract and exert tension on the surrounding matrix. This aligns with another study by Burger et al. exploring the consequence of FBLN4 deficiency on cytoskeletal structure and dynamics, revealing that FBLN4 is required for actin stress fiber formation.[68] We observed that FBLN4 and LTBP4 promoted enhanced focal adhesion formation, maturation, and increased pFAK levels. Focal adhesion formation is one of the important downstream events after cell interactions with several ECM proteins involved in elastogenesis, including fibronectin[69–71] and fibrillin-1,[72] albeit those are primarily integrin-mediated and relatively little is known about syndecans in this context.[73] One notable example is that SDC2 has been shown to function independently of integrins to induce FAK phosphorylation and elevate

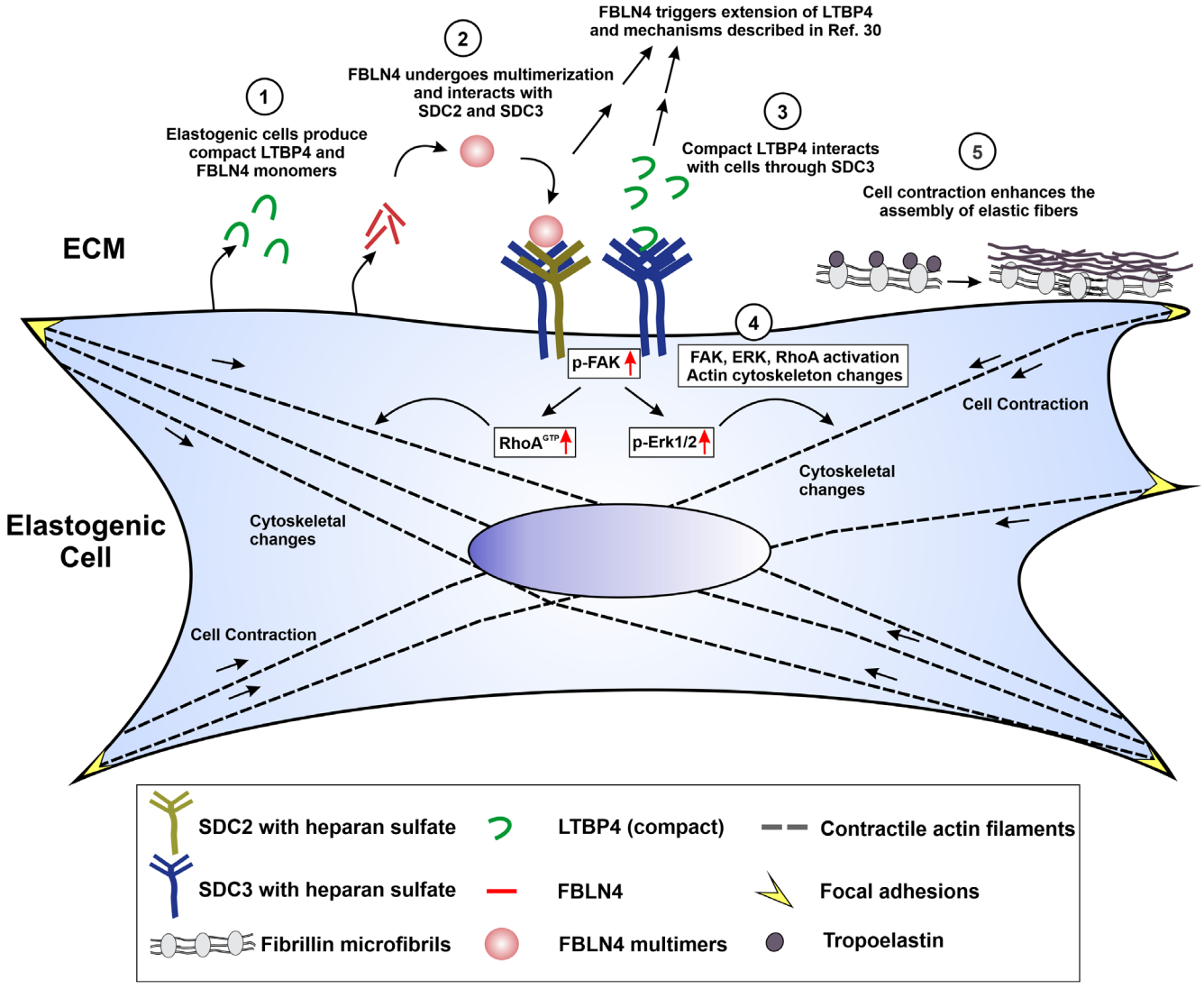

FIGURE 12 Role of FBLN4 and LTBP4 cell interactions in elastogenesis. Schematic summary of the findings in this study regarding FBLN4 and LTBP4 cell interactions and their involvement in elastogenesis. Details are described in the main text. Note that this proposed model positions additional aspects into the existing molecular framework of elastogenesis as we have described previously.[30] For simplicity, several aspects of the previously described model are not shown here. The various components in the figure are not drawn to scale.

ERK levels in cancer cells.[74] We found that cells seeded together with FBLN4 and LTBP4 in 3D cellularized collagen gels contracted more over time versus controls without FBLN4 and LTBP4. We also show that FBLN4- and LTBP4-elicited cell contraction is mediated by RhoA and ERK1/2 signaling. Both effectors are established promoters of cell contraction via the actin-myosin contractile system.[75–77] We established through FAK, ERK1/2, and RhoA inhibition that these effectors are essential for the regulation of elastic fiber formation. Additionally, inhibition of actin-myosin contractility using blebbistatin also led to impaired elastic fiber assembly. All data together are consistent with the interpretation that both FBLN4 and LTBP4 promote elastogenesis through SDC2 and SDC3 by initiating cell contraction via FAK, ERK1/2, and RhoA signaling. It remains to be experimentally established how cellular contractility promotes downstream the formation of elastic fibers. In this context, a previous study has shown that cell and extracellular matrix movements are essential for the aggregation and formation of elastic fibers.[78] Actin fibers also connect to integrins through focal adhesions, which in turn link to the extracellular matrix. Notably, integrins αvβ5 and αvβ3 have been shown to directly interact with the C-terminal and central domains of tropoelastin.[79–81] While our findings indicate that integrins are not required for direct cell interactions of FBLN4 and LTBP4, it is possible that the cytoskeletal changes and forces induced by these interactions could affect integrin-mediated connections with tropoelastin or other key scaffolding proteins, such as fibrillin-1 microfibrils.[82–84] For the formation of fibronectin fibers, it has been suggested that integrin α5β1-mediated contractile actin forces on the soluble fibronectin dimer trigger structural changes and network formation.[85,86] Possibly, similar mechanisms exist for the formation of elastic fibers.

Noda et al. demonstrated that FBLN4 can be internalized by cells via endocytosis and that intracellular FBLN4 is essential for the formation of lysine tyrosylquinone, a cofactor of the tropoelastin cross-linking enzyme LOX.[25] Even though the authors demonstrated in this work that FBLN4 was effectively internalized, they did not identify the responsible cell surface receptor. In light of our data, it is possible that SDC2 and/or SDC3 mediate endocytosis of FBLN4 for the purpose of intracellular lysine tyrosylquinone formation. This would further contribute to the stabilization of nascent elastic fibers.

In Figure 12, we provide a graphical working model emerging from our findings and building on our previous molecular model of elastogenesis,[30] whereby some aspects are hypothetical. (1) Elastogenic cells such as fibroblasts or smooth muscle cells produce FBLN4 and compact LTBP4. (2) FBLN4 undergoes self-interaction and forms multimers that interact with SDC2 and SDC3 on the cell surface. (3) LTBP4 interacts in its compact form with cells through SDC3. (4) These interactions trigger changes in the actin cytoskeleton by activating FAK, ERK, and RhoA, resulting in cell contraction. (5) Enhanced contractility promotes increased elastogenesis in the ECM. At a currently undetermined stage, FBLN4 interacts with LTBP4, which triggers the extension of the compact LTBP4, leading to the subsequent molecular mechanism described previously (not shown for simplicity).[30]

AUTHOR CONTRIBUTIONS

HH and DPR conceived the study, designed the experiments, and analyzed the data. HH and NEHD performed the experiments. HH, NEHD, and DPR wrote and edited the manuscript (with critical input from all authors). VN provided various methodological contributions. NLV and SRB provided reagents and critical input for the study. DPR acquired the funding.

ACKNOWLEDGMENTS

This study was supported by the Genetic Aortic Disorders Association Canada (Gada Canada Aortic Research Grant Award 2024 to DPR), the Natural Sciences and Engineering Research Council of Canada (RGPIN-2022-05045 to DPR), King Saud University, Riyadh–Saudi Arabia (Fellowship to HH), the Embassy of the Kingdom of Saudi Arabia in Canada (Operating funds to HH), and the Fonds de recherche de Quebec (Dossier No. 291220, fellowship to NEHD). We thank Yizhou Zhao for extensive help with the generation of LTBP4 recombinant plasmids and proteins, Dr. Frank Gondelaud for the generation of the syndecan recombinant plasmids, and Dr. Rongmo Zhang for expert contributions to immunofluorescence analyses.

DISCLOSURES

The authors declare no conflicts of interest.

DATA AVAILABILITY STATEMENT

The data sets of this study are available from the corresponding author upon request.

ORCID

Sylvie Ricard-Blum https://orcid.org/0000-0001-9263-1851
Dieter P. Reinhardt https://orcid.org/0000-0001-6535-9872

REFERENCES

1. Mecham RP. Elastin in lung development and disease pathogenesis. *Matrix Biol*. 2018;73:6-20.
2. Ross R, Bornstein P. The elastic fiber: the separation and partial characterization of its macromolecular components. *J Cell Biol*. 1969;40:366-381.

3. Sakai LY, Keene DR, Engvall E. Fibrillin, a new 350-kD glycoprotein, is a component of extracellular microfibrils. *J Cell Biol*. 1986;103:2499-2509.
4. Kozel BA, Rongish BJ, Czirok A, et al. Elastic fiber formation: a dynamic view of extracellular matrix assembly using timer reporters. *J Cell Physiol*. 2006;207:87-96.
5. Halm M, Schenke-Layland K, Jaspers S, Wenck H, Fischer F. Visualizing tropoelastin in a long-term human elastic fibre cell culture model. *Sci Rep*. 2016;6:20378.
6. Papke CL, Yanagisawa H. Fibulin-4 and fibulin-5 in elastogenesis and beyond: insights from mouse and human studies. *Matrix Biol*. 2014;37:142-149.
7. Pilecki B, Holm AT, Schlosser A, et al. Characterization of microfibrillar-associated Protein 4 (MFAP4) as a tropoelastin- and fibrillin-binding protein involved in elastic fiber formation. *J Biol Chem*. 2016;291:1103-1114.
8. Sato F, Seino-Sudo R, Okada M, Sakai H, Yumoto T, Wachi H. Lysyl oxidase enhances the deposition of tropoelastin through the catalysis of tropoelastin molecules on the cell surface. *Biol Pharm Bull*. 2017;40:1646-1653.
9. Zanetti M, Braghetta P, Sabatelli P, et al. EMILIN-1 deficiency induces elastogenesis and vascular cell defects. *Mol Cell Biol*. 2004;24:638-650.
10. Giltay R, Timpl R, Kostka G. Sequence, recombinant expression and tissue localization of two novel extracellular matrix proteins, fibulin-3 and fibulin-4. *Matrix Biol*. 1999;18:469-480.
11. Giltay R, Kostka G, Timpl R. Sequence and expression of a novel member (LTBP-4) of the family of latent transforming growth factor-beta binding proteins. *FEBS Lett*. 1997;411:164-168.
12. Saharinen J, Taipale J, Monni O, Keski-Oja J. Identification and characterization of a new latent transforming growth factor-beta-binding protein, LTBP-4. *J Biol Chem*. 1998;273:18459-18469.
13. Koli K, Hyytiäinen M, Ryynanen MJ, Keski-Oja J. Sequential deposition of latent TGF-beta binding proteins (LTBPs) during formation of the extracellular matrix in human lung fibroblasts. *Exp Cell Res*. 2005;310(2):370-382. doi:10.1016/j.yexcr.2005.08.008
14. Dasouki M, Markova D, Garola R, et al. Compound heterozygous mutations in fibulin-4 causing neonatal lethal pulmonary artery occlusion, aortic aneurysm, arachnodactyly, and mild cutis laxa. *Am J Med Genet A*. 2007;143A:2635-2641.
15. Renard M, Holm T, Veith R, et al. Altered TGFbeta signaling and cardiovascular manifestations in patients with autosomal recessive cutis laxa type I caused by fibulin-4 deficiency. *Eur J Hum Genet*. 2010;18:895-901.
16. Hebson C, Coleman K, Clabby M, et al. Severe aortopathy due to fibulin-4 deficiency: molecular insights, surgical strategy, and a review of the literature. *Eur J Pediatr*. 2014;173:671-675.
17. Hucthagowder V, Sausgruber N, Kim KH, Angle B, Marmorstein LY, Urban Z. Fibulin-4: a novel gene for an autosomal recessive cutis laxa syndrome. *Am J Hum Genet*. 2006;78:1075-1080.
18. Hanada K, Vermeij M, Garinis GA, et al. Perturbations of vascular homeostasis and aortic valve abnormalities in fibulin-4 deficient mice 1. *Circ Res*. 2007;100:738-746.
19. McLaughlin PJ, Chen Q, Horiguchi M, et al. Targeted disruption of fibulin-4 abolishes elastogenesis and causes perinatal lethality in mice. *Mol Cell Biol*. 2006;26(5):1700-1709. doi:10.1128/MCB.26.5.1700-1709.2006
20. Urban Z, Hucthagowder V, Schurmann N, et al. Mutations in LTBP4 cause a syndrome of impaired pulmonary, gastrointestinal, genitourinary, musculoskeletal, and dermal development. *Am J Hum Genet*. 2009;85:593-605.
21. Callewaert B, Su CT, Van Damme T, et al. Comprehensive clinical and molecular analysis of 12 families with type 1 recessive cutis laxa. *Hum Mutat*. 2013;34:111-121.
22. Urban Z, Davis EC. Cutis laxa: intersection of elastic fiber biogenesis, TGFbeta signaling, the secretory pathway and metabolism. *Matrix Biol*. 2014;33:16-22.
23. Dabovic B, Robertson IB, Zilberberg L, Vassallo M, Davis EC, Rifkin DB. Function of latent TGFbeta binding protein 4 and fibulin 5 in elastogenesis and lung development. *J Cell Physiol*. 2015;230:226-236.
24. Bultmann-Mellin I, Conradi A, Maul AC, et al. Modeling autosomal recessive cutis laxa type 1C in mice reveals distinct functions for Ltbp-4 isoforms. *Dis Model Mech*. 2015;8:403-415.
25. Noda K, Kitagawa K, Miki T, et al. A matricellular protein fibulin-4 is essential for the activation of lysyl oxidase. *Sci Adv*. 2020;6:eabc1404.
26. Horiguchi M, Inoue T, Ohbayashi T, et al. Fibulin-4 conducts proper elastogenesis via interaction with cross-linking enzyme lysyl oxidase. *Proc Natl Acad Sci USA*. 2009;106(45):19029-19034. doi:10.1073/pnas.0908268106
27. Choudhury R, McGovern A, Ridley C, et al. Differential regulation of elastic fiber formation by fibulins-4 and -5. *J Biol Chem*. 2009;284:24553-24567.
28. El-Hallous E, Sasaki T, Hubmacher D, et al. Fibrillin-1 interactions with fibulins depend on the first hybrid domain and provide an adapter function to tropoelastin. *J Biol Chem*. 2007;282:8935-8946.
29. Kobayashi N, Kostka G, Garbe JH, et al. A comparative analysis of the fibulin protein family. Biochemical characterization, binding interactions, and tissue localization. *J Biol Chem*. 2007;282:11805-11816.
30. Kumra H, Nelea V, Hakami H, et al. Fibulin-4 exerts a dual role in LTBP-4L-mediated matrix assembly and function. *Proc Natl Acad Sci USA*. 2019;116:20428-20437.
31. Noda K, Dabovic B, Takagi K, et al. Latent TGF-beta binding protein 4 promotes elastic fiber assembly by interacting with fibulin-5. *Proc Natl Acad Sci USA*. 2013;110:2852-2857.
32. Djokic J, Fagotto-Kaufmann C, Bartels R, Nelea V, Reinhardt DP. Fibulin-3, −4, and −5 are highly susceptible to proteolysis, interact with cells and heparin, and form multimers. *J Biol Chem*. 2013;288:22821-22835.
33. Kantola AK, Keski-Oja J, Koli K. Fibronectin and heparin binding domains of latent TGF-beta binding protein (LTBP)-4 mediate matrix targeting and cell adhesion. *Exp Cell Res*. 2008;314:2488-2500.
34. Couchman JR, Gopal S, Lim HC, Norgaard S, Multhaupt HA. Syndecans: from peripheral coreceptors to mainstream regulators of cell behaviour. *Int J Exp Pathol*. 2015;96:1-10.
35. Woods A. Syndecans: transmembrane modulators of adhesion and matrix assembly. *J Clin Invest*. 2001;107:935-941.
36. Ricard-Blum S, Couchman JR. Conformations, interactions and functions of intrinsically disordered syndecans. *Biochem Soc Trans*. 2023;51:1083-1096.
37. Gopal S, Couchman J, Pocock R. Redefining the role of syndecans in *C. elegans* biology. *Worm*. 2016;5:e1142042.
38. Dews IC, Mackenzie KR. Transmembrane domains of the syndecan family of growth factor coreceptors display a hierarchy

of homotypic and heterotypic interactions. *Proc Natl Acad Sci USA*. 2007;104:20782-20787.
39. Reinhardt DP, Ono RN, Notbohm H, Müller PK, Bächinger HP, Sakai LY. Mutations in calcium-binding epidermal growth factor modules render fibrillin-1 susceptible to proteolysis: a potential disease-causing mechanism in Marfan syndrome. *J Biol Chem*. 2000;275:12339-12345.
40. Zeyer KA, Zhang RM, Kumra H, Hassan A, Reinhardt DP. The fibrillin-1 RGD integrin binding site regulates gene expression and cell function through microRNAs. *J Mol Biol*. 2019;431:401-421.
41. Reinhardt DP, Gambee JE, Ono RN, Bächinger HP, Sakai LY. Initial steps in assembly of microfibrils. Formation of disulfide-cross-linked multimers containing fibrillin-1. *J Biol Chem*. 2000;275(3):2205-2210. doi:10.1074/jbc.275.3.2205
42. Hakami H. *Identification of the cell receptors for fibulin-4 and latent transforming growth factor-β binding protein-4, and their functional roles in elastogenesis*. PhD thesis. McGill University; 2021.
43. Tiedemann K, Bätge B, Müller PK, Reinhardt DP. Interactions of fibrillin-1 with heparin/heparan sulfate: implications for microfibrillar assembly. *J Biol Chem*. 2001;276:36035-36042.
44. Zhang R, Kumra H, Reinhardt DP. Quantification of extracellular matrix fiber systems related to ADAMTS proteins. *Methods Mol Biol*. 2020;2043:237-250.
45. Schneider CA, Rasband WS, Eliceiri KW. NIH image to ImageJ: 25 years of image analysis. *Nat Methods*. 2012;9:671-675.
46. Horzum U, Ozdil B, Pesen-Okvur D. Step-by-step quantitative analysis of focal adhesions. *MethodsX*. 2014;1:56-59.
47. Kumra H, Sabatier L, Hassan A, et al. Roles of fibronectin isoforms in neonatal vascular development and matrix integrity. *PLoS Biol*. 2018;16:e2004812.
48. Xiong JP, Stehle T, Goodman SL, Arnaout MA. Integrins, cations and ligands: making the connection. *J Thromb Haemost*. 2003;1:1642-1654.
49. Gondelaud F, Ricard-Blum S. Structures and interactions of syndecans. *FEBS J*. 2019;286:2994-3007.
50. Klass CM, Couchman JR, Woods A. Control of extracellular matrix assembly by syndecan-2 proteoglycan. *J Cell Sci*. 2000;113:493-506.
51. Tumova S, Woods A, Couchman JR. Heparan sulfate proteoglycans on the cell surface: versatile coordinators of cellular functions. *Int J Biochem Cell Biol*. 2000;32:269-288.
52. Woods A, Longley RL, Tumova S, Couchman JR. Syndecan-4 binding to the high affinity heparin-binding domain of fibronectin drives focal adhesion formation in fibroblasts. *Arch Biochem Biophys*. 2000;374:66-72.
53. Lyon M, Rushton G, Askari JA, Humphries MJ, Gallagher JT. Elucidation of the structural features of heparan sulfate important for interaction with the Hep-2 domain of fibronectin. *J Biol Chem*. 2000;275:4599-4606.
54. Tapon N, Hall A. Rho, Rac and Cdc42 GTPases regulate the organization of the actin cytoskeleton. *Curr Opin Cell Biol*. 1997;9:86-92.
55. Raftopoulou M, Hall A. Cell migration: rho GTPases lead the way. *Dev Biol*. 2004;265:23-32.
56. Ridley AJ, Hall A. The small GTP-binding protein rho regulates the assembly of focal adhesions and actin stress fibers in response to growth factors. *Cell*. 1992;70:389-399.
57. Nobes CD, Hall A. Rho, rac and cdc42 GTPases: regulators of actin structures, cell adhesion and motility. *Biochem Soc Trans*. 1995;23:456-459.
58. Machesky LM. Cell motility: complex dynamics at the leading edge. *Curr Biol*. 1997;7:R164-R167.
59. Ilic D, Kovacic B, Johkura K, et al. FAK promotes organization of fibronectin matrix and fibrillar adhesions. *J Cell Sci*. 2004;117:177-187.
60. Oeckler RA, Kaminski PM, Wolin MS. Stretch enhances contraction of bovine coronary arteries via an NAD(P)H oxidase-mediated activation of the extracellular signal-regulated kinase mitogen-activated protein kinase cascade. *Circ Res*. 2003;92:23-31.
61. Dessy C, Kim I, Sougnez CL, Laporte R, Morgan KG. A role for MAP kinase in differentiated smooth muscle contraction evoked by alpha-adrenoceptor stimulation. *Am J Phys*. 1998;275(4):C1081-C1086. doi:10.1152/ajpcell.1998.275.4.C1081
62. Tong J, Li L, Ballermann B, Wang Z. Phosphorylation and activation of RhoA by ERK in response to epidermal growth factor stimulation. *PLoS One*. 2016;11(1):e0147103. doi:10.1371/journal.pone.0147103
63. Straight AF, Cheung A, Limouze J, et al. Dissecting temporal and spatial control of cytokinesis with a myosin II inhibitor. *Science*. 2003;299:1743-1747.
64. Votteler M, Berrio DA, Horke A, et al. Elastogenesis at the onset of human cardiac valve development. *Development*. 2013;140(11):2345-2353. doi:10.1242/dev.093500
65. Hubmacher D, El-Hallous E, Nelea V, Kaartinen MT, Lee ER, Reinhardt DP. Biogenesis of extracellular microfibrils: multimerization of the fibrillin-1 C-terminus into bead-like structures enables self-assembly. *Proc Natl Acad Sci USA*. 2008;105:6548-6553.
66. Rifkin DB. Latent transforming growth factor-beta (TGF-beta) binding proteins: orchestrators of TGF-beta availability. *J Biol Chem*. 2005;280:7409-7412.
67. Saharinen J, Keski-Oja J. Specific sequence motif of 8-Cys repeats of TGF-beta binding proteins, LTBPs, creates a hydrophobic interaction surface for binding of small latent TGF-beta. *Mol Biol Cell*. 2000;11:2691-2704.
68. Burger J, van Vliet N, van Heijningen P, et al. Fibulin-4 deficiency differentially affects cytoskeleton structure and dynamics as well as TGFbeta signaling. *Cell Signal*. 2019;58:65-78.
69. Zhong C, Chrzanowska-Wodnicka M, Brown J, Shaub A, Belkin AM, Burridge K. Rho-mediated contractility exposes a cryptic site in fibronectin and induces fibronectin matrix assembly. *J Cell Biol*. 1998;141:539-551.
70. Hocking DC, Smith RK, McKeown-Longo PJ. A novel role for the integrin-binding III-10 module in fibronectin matrix assembly. *J Cell Biol*. 1996;133(2):431-444. doi:10.1083/jcb.133.2.431
71. Dzamba BJ, Bultmann H, Akiyama SK, Peters DM. Substrate-specific binding of the amino terminus of fibronectin to an integrin complex in focal adhesions. *J Biol Chem*. 1994;269:19646-19652.
72. Bax DV, Mahalingam Y, Cain S, et al. Cell adhesion to fibrillin-1: identification of an Arg-Gly-Asp-dependent synergy region and a heparin-binding site that regulates focal adhesion formation. *J Cell Sci*. 2007;120:1383-1392.
73. Lambaerts K, Wilcox-Adelman SA, Zimmermann P. The signaling mechanisms of syndecan heparan sulfate proteoglycans. *Curr Opin Cell Biol*. 2009;21:662-669.

74. Jang B, Jung H, Choi S, Lee YH, Lee ST, Oh ES. Syndecan-2 cytoplasmic domain up-regulates matrix metalloproteinase-7 expression via the protein kinase Cgamma-mediated FAK/ERK signaling pathway in colon cancer. *J Biol Chem*. 2017;292:16321-16332.
75. Nunes KP, Webb RC. New insights into RhoA/Rho-kinase signaling: a key regulator of vascular contraction. *Small GTPases*. 2021;12:458-469.
76. Zhang W, Huang Y, Gunst SJ. The small GTPase RhoA regulates the contraction of smooth muscle tissues by catalyzing the assembly of cytoskeletal signaling complexes at membrane adhesion sites. *J Biol Chem*. 2012;287:33996-34008.
77. Ihara E, Yu Q, Chappellaz M, MacDonald JA. ERK and p38MAPK pathways regulate myosin light chain phosphatase and contribute to Ca2+ sensitization of intestinal smooth muscle contraction. *Neurogastroenterol Motil*. 2015;27:135-146.
78. Czirok A, Zach J, Kozel BA, Mecham RP, Davis EC, Rongish BJ. Elastic fiber macro-assembly is a hierarchical, cell motion-mediated process. *J Cell Physiol*. 2006;207:97-106.
79. Rodgers UR, Weiss AS. Integrin alpha v beta 3 binds a unique non-RGD site near the C-terminus of human tropoelastin. *Biochimie*. 2004;86:173-178.
80. Bax DV, Rodgers UR, Bilek MM, Weiss AS. Cell adhesion to tropoelastin is mediated via the C-terminal GRKRK motif and integrin alphaVbeta3. *J Biol Chem*. 2009;284:28616-28623.
81. Lee P, Bax DV, Bilek MM, Weiss AS. A novel cell adhesion region in tropoelastin mediates attachment to integrin alphaVbeta5. *J Biol Chem*. 2014;289:1467-1477.
82. Pfaff M, Reinhardt DP, Sakai LY, Timpl R. Cell adhesion and integrin binding to recombinant human fibrillin-1. *FEBS Lett*. 1996;384:247-250.
83. Sakamoto H, Broekelmann T, Cheresh DA, Ramirez F, Rosenbloom J, Mecham RP. Cell-type specific recognition of RGD- and non-RGD-containing cell binding domains in fibrillin-1. *J Biol Chem*. 1996;271:4916-4922.
84. Bax DV, Bernard SE, Lomas A, et al. Cell adhesion to fibrillin-1 molecules and microfibrils is mediated by alpha5 beta1 and alphav beta3 integrins. *J Biol Chem*. 2003;278:34605-34616.
85. Singh P, Carraher C, Schwarzbauer JE. Assembly of fibronectin extracellular matrix. *Annu Rev Cell Dev Biol*. 2010;26:397-419.
86. Fogerty FJ, Akiyama SK, Yamada KM, Mosher DF. Inhibition of binding of fibronectin to matrix assembly sites by anti-integrin (alpha 5 beta 1) antibodies. *J Cell Biol*. 1990;111:699-708.

SUPPORTING INFORMATION

Additional supporting information can be found online in the Supporting Information section at the end of this article.

How to cite this article: Hakami H, Dinesh NEH, Nelea V, Lamarche-Vane N, Ricard-Blum S, Reinhardt DP. Fibulin-4 and latent-transforming growth factor beta-binding protein-4 interactions with syndecan-2 and syndecan-3 are required for elastogenesis. *The FASEB Journal*. 2025;39:e70505. doi:10.1096/fj.202402767R